The $1 : \sqrt{2}$ Hopf/steady-state mode interaction in three-dimensional magnetoconvection

J. H. P. Dawes

Department of Applied Mathematics and Theoretical Physics, University of Cambridge, Silver Street, Cambridge, CB3 9EW, UK. Tel: +44-1223-337900. Fax: +44-1223-337918. Email: J.H.P.Dawes@damtp.cam.ac.uk

Abstract

The first analysis of a properly three-dimensional mode interaction between steady and oscillatory forms of convection with different preferred wavenumbers is presented. By varying the fluid parameters for Boussinesq magnetoconvection we locate a point where the conduction state is unstable to both steady and oscillatory motion simultaneously. We then construct and analyse the normal form. The complex transition between steady and oscillatory convection near onset can be explained: this extends and completes the work of Clune and Knobloch [1]. Selecting the most marginal wavenumbers in the problem ensures that the analysis is relevant to the behaviour which would be observed in an unbounded plane layer.

The symmetries of the resulting $D_4 \ltimes T^2$-equivariant bifurcation problem play a large role in determining the bifurcation structure and explain the appearance of interesting phenomena such as drifting solutions [2]. We also find new phenomena in the normal form for a Hopf bifurcation with $D_4 \ltimes T^2$ symmetry [3].

The introduction of weakly non-Boussinesq effects leads to qualitative changes in the dynamics near onset: different convection planforms are stabilised and chaotic heteroclinic cycling behaviour is observed.

Key words: mode interaction, drifting solutions, 3D magnetoconvection.
PACS Codes: 47.54; 47.20; 47.65

1 Introduction

Steady-state/steady-state and Hopf/steady-state mode interactions have been widely studied in two-dimensional convection [4,5], as have Takens-Bogdanov bifurcations [6,7]. In a three-dimensional problem these interactions still occur but in all cases the modes may be unstable to three-dimensional perturbations.

More recently there has been an interest in mode interactions which are truly three-dimensional. The interaction of two steady modes at 45° to each other with wavenumbers in the ratio $1 : \sqrt{2}$ was studied by Proctor and Matthews [8] as a possible explanation for subcritical square-cell convection in experiments on a fluid with variable viscosity. Also, Renardy, Renardy and Fujimura [9] have studied a Takens-Bogdanov bifurcation on a hexagonal lattice with applications to a two-layer convection problem.

We study a new interaction of steady and oscillatory behaviour which occurs in magnetoconvection with a vertical magnetic field. The interaction takes place when we vary the fluid parameters so that the trivial conduction state is simultaneously unstable to both forms of convection. By varying the fluid parameters we can also fix the wavenumbers of these modes to be in the ratio $1 : \sqrt{2}$, enabling us to restrict our attention to those modes which lie on a periodic square lattice in the plane. This restriction, which makes the centre manifold finite dimensional, allows us to derive a set of amplitude equations for the dynamics on the centre manifold. The amplitude equations are the truncation at cubic order of the normal form for this mode interaction with $D_4 \ltimes T^2$ symmetry. They are an asymptotically exact model of the behaviour of the fluid at the onset of convection in the neighbourhood of the $1 : \sqrt{2}$ resonance; this leads to a codimension 2 bifurcation problem. As we also require the resonant modes to be the most unstable ones we actually impose four conditions on the physical parameters of the problem, but as the resulting ODEs contain only two bifurcation parameters it is better described as a codimension 2 problem rather than a codimension 4 one.

The preferred planform for Boussinesq magnetoconvection at onset has been studied in detail by Clune and Knobloch [1]. Their analysis does not, however, explain how a smooth transition from steady to oscillatory convection can occur. Although there is a jump in the most unstable wavenumber, a two-parameter unfolding (as we give here) can provide that explanation and complete their analysis.

Using modified perturbation theory we can evaluate the coefficients in this normal form at the codimension 2 point. For a Boussinesq fluid we can draw on earlier work [3] to help analyse the dynamics in two invariant subspaces in the problem; the bifurcation structure is complex, and shows the existence of chaotic solutions arbitrarily close to onset. The weakly non-Boussinesq analysis is extremely complex, and here we restrict the analysis to two contrasting cases and point out their interesting features. At all times we will concentrate on stable objects in the bifurcation structure as only these will be physically relevant.

The relevant coefficient values also highlight previously unseen behaviour in the analysis of a Hopf bifurcation with $D_4 \ltimes T^2$ symmetry [3]; this is examined

in more detail in [10].

The initial conduction solution planform is invariant under the group $E(2)$ of all Euclidean symmetries of the plane $\mathbb{R}^2$. By then restricting our attention to solutions which lie on a square lattice the problem becomes a mode interaction with $D_4 \ltimes T^2$ symmetry. The possible bifurcations from a given solution are organised by its symmetry group [13]; it is important to understand the role of the spatial and spatiotemporal symmetries. Novel solutions are found which drift slowly in space and we explain why this is possible. The spatiotemporal structure of these planforms can best be appreciated by viewing animations.

In section 2 we provide the fluid-dynamical background for the problem and in section 3 we derive the normal form equations for the mode interaction. Section 4 contains a discussion of the Boussinesq behaviour and the use of symmetries in classifying bifurcations. Aspects of the non-Boussinesq behaviour are presented in section 5 and we draw conclusions in section 6.

2 Physical Background

Boussinesq magnetoconvection in a uniform vertical magnetic field with stress-free, fixed temperature upper and lower boundaries and periodic lateral boundaries has been extensively investigated [11]. After the governing equations have been nondimensionalised there are four dimensionless parameters: the Prandtl number $\sigma = \nu/\kappa$ (the ratio of the rates at which velocity and temperature gradients diffuse), the magnetic Prandtl number $\zeta = \nu/\eta$ (the ratio of the rates at which velocity and magnetic flux gradients diffuse), the Chandrasekhar number Q which is proportional to the square of the magnetic field strength and the Rayleigh number R which is proportional to the temperature difference between the top and bottom of the fluid layer.

The governing nondimensionalised equations for perturbations to the conduction solution $\mathbf{u}_{cond} = 0$, $\mathbf{B}_{cond} = \hat{\mathbf{z}}$, $T_{cond} = 1 - z$ in three dimensions are the (curl of the) momentum equation, the induction equation and the heat transfer equation:

$$\partial_t \boldsymbol{\omega} + \nabla \times (\boldsymbol{\omega} \times \mathbf{u}) = \sigma\zeta Q\left[\nabla \times (\mathbf{J} \times \mathbf{B}) + \partial_z \mathbf{J}\right] + R\sigma \nabla \times (T\hat{\mathbf{z}}) + \sigma \nabla^2 \boldsymbol{\omega} \tag{1}$$

$$\partial_t \mathbf{B} + \nabla \times (\mathbf{B} \times \mathbf{u}) = \partial_z \mathbf{u} + \zeta \nabla^2 \mathbf{B} \tag{2}$$

$$\partial_t T + \mathbf{u} \cdot \nabla T = u_z + \nabla^2 T \tag{3}$$

where $\mathbf{J} = \nabla \times \mathbf{B}$ and $\boldsymbol{\omega} = \nabla \times \mathbf{u}$, and by taking the curl of the momentum equation we have eliminated the pressure term. The velocity field $\mathbf{u} = (u_x, u_y, u_z)$

and the magnetic field perturbation $\mathbf{B} = (B_x, B_y, B_z)$ are both solenoidal: $\nabla \cdot \mathbf{u} = \nabla \cdot \mathbf{B} = 0$. The (stress-free) boundary conditions are

$$\partial_z u_x = \partial_z u_y = u_z = B_x = B_y = \partial_z B_z = T = 0 \quad \text{at} \quad z = 0 \quad \text{and} \quad z = 1 \tag{4}$$

To find the $1 : \sqrt{2}$ resonance point we vary the parameters so that the transitions to oscillatory and steady convection happen at the same critical Rayleigh number, and the wavenumber of the oscillatory convection is lower by a factor of $\sqrt{2}$ than that of the steady modes. This can be done from 2D linear theory (see [11]): for steady convection at a wavenumber α_s the critical Rayleigh number R_s is found to be

$$R_s = \frac{(\alpha_s^2 + \pi^2)^3}{\alpha_s^2} + \frac{Q\pi^2(\alpha_s^2 + \pi^2)}{\alpha_s^2} \tag{5}$$

For oscillatory convection at wavenumber α_o the critical Rayleigh number R_o is similarly found to be (assuming $\zeta < 1$):

$$R_o = \frac{(\alpha_o^2 + \pi^2)^3}{\alpha_o^2} C_1 + \frac{Q\pi^2(\alpha_o^2 + \pi^2)}{\alpha_o^2} C_2 \tag{6}$$

where $C_1 = (\sigma + \zeta)(1 + \zeta)/\sigma$ and $C_2 = (\sigma + \zeta)\zeta/(1 + \sigma)$ are constants. The preferred wavenumber for the onset of either form of convection occurs where R is a minimum. We also require that the wavenumbers α_o and α_s which minimise R_o and R_s must be in the ratio $1 : \sqrt{2}$ and that the critical Rayleigh numbers at these wavenumbers must be equal. These conditions lead to the following equations.

$$2\alpha_o^6 + 3\pi^2\alpha_o^4 - \pi^6 - \frac{Q\pi^4 C_2}{C_1} = 0 \tag{7}$$

$$2\alpha_s^6 + 3\pi^2\alpha_s^4 - \pi^6 - \pi^4 Q = 0 \tag{8}$$

$$\frac{(\alpha_s^2 + \pi^2)^3}{\alpha_s^2} + \frac{Q\pi^2(\alpha_s^2 + \pi^2)}{\alpha_s^2} = \frac{(\alpha_o^2 + \pi^2)^3}{\alpha_o^2} C_1 + \frac{Q\pi^2(\alpha_o^2 + \pi^2)}{\alpha_o^2} C_2 \tag{9}$$

$$\alpha_o^2 = \alpha_s^2/2 \tag{10}$$

This is a system of four equations in five unknowns (α_s, α_o, Q, σ, and ζ). By fixing one parameter (here we fix ζ) we can solve numerically for the other four. Fixing ζ at values $0.1, 0.2, \ldots, 0.9$ and solving for the other parameter values gives the results shown in table 1. ω_0 is the frequency of oscillation at onset for the oscillatory modes. From linear theory this is given by:

Table 1
The position of the $1:\sqrt{2}$ point with varying ζ.

ζ	σ	Q	α_s^2	$R_c = R_s = R_o$	ω_0
0.1	0.0855	41.0485	9.9992	1589.44	0.8139
0.2	0.1944	46.1929	10.4069	1689.32	1.6693
0.3	0.3192	56.4837	11.1571	1883.84	2.6175
0.4	0.4445	75.7488	12.3844	2233.33	3.7335
0.5	0.5475	113.5690	14.3581	2881.83	5.1454
0.6	0.6038	197.6955	17.6494	4223.06	7.1059
0.7	0.5987	431.1269	23.6374	7623.22	10.2059
0.8	0.5361	1397.1788	36.5353	20249.85	16.2283
0.9	0.4381	11377.4262	77.5103	135196.45	34.1120

$$\omega_0^2 = \frac{\pi^2\sigma\zeta Q(1-\zeta)}{1+\sigma} - \zeta^2(\alpha_o^2+\pi^2)^2 \tag{11}$$

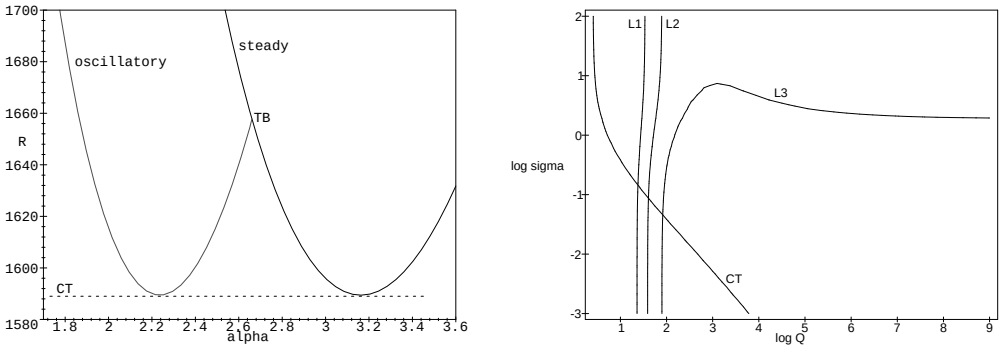

(a) (b)

Fig. 1. (a) The marginal stability curves for the onset of steady and oscillatory convection at a $1:\sqrt{2}$ point. The wavenumber α is plotted along the x-axis, and the Rayleigh number R along the y-axis. $\zeta = 0.1$, $\sigma = 0.0855$ and $Q = 41.0485$. TB denotes the Takens-Bogdanov point and the dashed line CT highlights the condition that the critical Rayleigh numbers are equal. (b) The CT line, and lines of constant $s = \alpha_s/\alpha_o$ in the (Q,σ) plane for $\zeta = 0.1$. L_1: $s = 1.3$, L_2: $s = \sqrt{2}$, L_3: $s = 1.6$. The lines CT and L_2 cross at the $1:\sqrt{2}$ point corresponding to the first line of table 1.

3 The Normal Form

To keep the centre manifold finite dimensional we restrict our possible solutions to those lying on a square lattice, choosing the lattice dimensions to match the most unstable wavenumber. This corresponds to the 'fundamental representation' of Dionne et al [12]. In this way we reduce the symmetries of the problem from $E(2)$ to the subgroup $D_4 \ltimes T^2$. This is the semi-direct product of two groups: D_4 is the group of the rotations and reflections of a square, and T^2 is the group of translations in the plane - the spatial origin of the lattice is not predetermined. We can describe the interactions between the steady and oscillatory modes by writing down a normal form for the evolution of the (complex) mode amplitudes. This leads to a set of six coupled equations for the amplitudes; two amplitudes describe the evolution of steady diagonal rolls and four more describe the oscillatory modes (travelling waves) in the $\pm x$ and $\pm y$ directions. The form of the equations is determined by requiring the equations to be equivariant with respect to the group $D_4 \ltimes T^2$.

The centre manifold is spanned by these six complex amplitudes, and so the planform (as described by a 'marker quantity' such as the vertical fluid velocity at the mid-plane) looks like

$$\begin{aligned} u_z(x,y,t) = Re(&A_1 e^{i(\alpha x - \omega_0 t)} + A_2 e^{-i(\alpha x + \omega_0 t)} + B_1 e^{i(\alpha y - \omega_0 t)} \\ &+ B_2 e^{-i(\alpha y + \omega_0 t)} + C e^{i\alpha(x+y)} + D e^{i\alpha(x-y)}) \end{aligned} \tag{12}$$

This is illustrated in figure 2. u_z must be equivariant under the symmetries

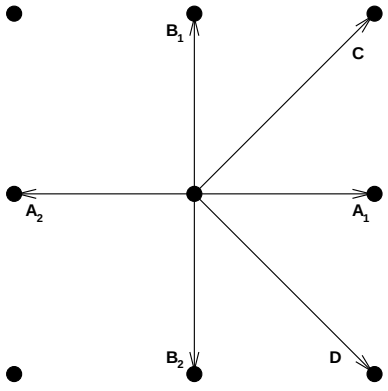

Fig. 2. The geometry of the planform.

$D_4 \ltimes T^2$, so the action of each symmetry on (x, y, t) induces an action on the mode amplitudes $\{A_1, A_2, B_1, B_2, C, D\}$:

Reflection in the y-axis

$$m_y : x \to -x : \quad A_1 \longleftrightarrow A_2 \quad B_1 \to B_1 \quad B_2 \to B_2 \quad C \longleftrightarrow \bar{D}$$

Reflection in the line $x = y$

$$m_d : x \longleftrightarrow y : \quad A_1 \longleftrightarrow B_1 \quad A_2 \longleftrightarrow B_2 \quad C \to C \quad D \to \bar{D}$$

Translation in the x and y directions:

$$\theta_x : x \to x + \delta/\alpha : \quad \{A_1, C, D\} \to \{A_1, C, D\}e^{i\delta} \quad \{B_1, B_2\} \to \{B_1, B_2\}$$
$$A_2 \to A_2 e^{-i\delta}$$

$$\theta_y : y \to y + \delta/\alpha : \quad \{A_1, A_2\} \to \{A_1, A_2\} \quad \{B_1, C\} \to \{B_1, C\}e^{i\delta}$$
$$\{B_2, D\} \to \{B_2, D\}e^{-i\delta}$$

The two reflections generate the group D_4 and the two translations generate the group T^2. Requiring equivariance with respect to these symmetries leads to the following system of ODEs (truncated at third order) for the six complex amplitudes.

$$\begin{aligned}\dot{A}_1 = {} & \mu_1 A_1 + \alpha_1(CB_2 + DB_1) + \alpha_2 \bar{A}_2 B_1 B_2 + \alpha_3 A_2 CD \\ & + A_1[\lambda_1|A_1|^2 + \lambda_2|A_2|^2 + \lambda_3(|B_1|^2 + |B_2|^2) + \lambda_4(|C|^2 + |D|^2)] \end{aligned} \tag{13}$$

$$\begin{aligned}\dot{A}_2 = {} & \mu_1 A_2 + \alpha_1(\bar{D}B_2 + \bar{C}B_1) + \alpha_2 \bar{A}_1 B_1 B_2 + \alpha_3 A_1 \bar{C}\bar{D} \\ & + A_2[\lambda_1|A_2|^2 + \lambda_2|A_1|^2 + \lambda_3(|B_1|^2 + |B_2|^2) + \lambda_4(|C|^2 + |D|^2)] \end{aligned} \tag{14}$$

$$\begin{aligned}\dot{B}_1 = {} & \mu_1 B_1 + \alpha_1(CA_2 + \bar{D}A_1) + \alpha_2 \bar{B}_2 A_1 A_2 + \alpha_3 B_2 C\bar{D} \\ & + B_1[\lambda_1|B_1|^2 + \lambda_2|B_2|^2 + \lambda_3(|A_1|^2 + |A_2|^2) + \lambda_4(|C|^2 + |D|^2)] \end{aligned} \tag{15}$$

$$\begin{aligned}\dot{B}_2 = {} & \mu_1 B_2 + \alpha_1(DA_2 + \bar{C}A_1) + \alpha_2 \bar{B}_1 A_1 A_2 + \alpha_3 B_1 \bar{C}D \\ & + B_2[\lambda_1|B_2|^2 + \lambda_2|B_1|^2 + \lambda_3(|A_1|^2 + |A_2|^2) + \lambda_4(|C|^2 + |D|^2)] \end{aligned} \tag{16}$$

$$\begin{aligned}\dot{C} = {} & \mu_2 C + \nu_1(A_1\bar{B}_2 + B_1\bar{A}_2) + \nu_2(B_1\bar{B}_2 D + A_1\bar{A}_2\bar{D}) \\ & + C[\beta_1|C|^2 + \beta_2|D|^2 + \beta_3(|A_1|^2 + |B_1|^2) + \bar{\beta}_3(|A_2|^2 + |B_2|^2)] \end{aligned} \tag{17}$$

$$\begin{aligned}\dot{D} = {} & \mu_2 D + \nu_1(A_1\bar{B}_1 + B_2\bar{A}_2) + \nu_2(\bar{B}_1 B_2 C + A_1\bar{A}_2\bar{C}) \\ & + D[\beta_1|D|^2 + \beta_2|C|^2 + \beta_3(|A_1|^2 + |B_2|^2) + \bar{\beta}_3(|A_2|^2 + |B_1|^2)] \end{aligned} \tag{18}$$

The coefficients μ_2, β_1, β_2, ν_1 and ν_2 are forced to be real by symmetry, but all other coefficients will in general be complex. The bifurcation parameter $\mu_1 = \hat{\mu}_1 + i\tilde{\omega}(\hat{\mu}_1)$ where $\hat{\mu}_1$ and $\tilde{\omega}$ are real. The frequency of the bifurcating

solutions in the Hopf bifurcation is close to ω_0 near the bifurcation point $\hat{\mu}_1 = 0$. The normal form also picks up a symmetry S^1, corresponding to a translation in time:

$$\theta_t : t \to t + \tau/\omega : \quad \begin{array}{l} \{A_1, A_2, B_1, B_2\} \to \{A_1, A_2, B_1, B_2\} e^{-i\tau} \\ \{C, D\} \to \{C, D\} \end{array}$$

This symmetry is not a symmetry of the physical problem, but it appears naturally in all normal forms for problems involving a Hopf bifurcation. There is also the Boussinesq symmetry to consider. If the fluid is Boussinesq (and, as we assume throughout, the upper and lower boundary conditions are identical) then we require the amplitude equations to be equivariant with respect to reflection $z \to 1 - z$ about the midplane $z = 1/2$ (as the original PDEs have this symmetry):

$$m_z : z \to 1 - z : \quad \{A_1, A_2, B_1, B_2, C, D\} \to -\{A_1, A_2, B_1, B_2, C, D\} \tag{19}$$

This has the effect of removing the quadratic terms from the amplitude equations by forcing α_1 and ν_1 to be zero.

Lastly, the planform (12) is invariant under a spatiotemporal symmetry h if the planform oscillates periodically with period T:

$$h : \quad (x, y, t) \to (x + \pi/\alpha, y + \pi/\alpha, t + T/2) \tag{20}$$

corresponding to a translation of half a wavelength in the x and y directions followed by a translation of half an oscillation period.

3.1 Fixed points in the invariant subspaces

When we are dealing with a Boussinesq fluid the parameters α_1 and ν_1 must be zero. The amplitude equations now have two clear invariant subspaces; one where $C = D = 0$ which is denoted $\mathcal{S}_1$, and one denoted $\mathcal{S}_2$ where $A_1 = A_2 = B_1 = B_2 = 0$ ($\mathcal{S}_2$ is an invariant subspace for the non-Boussinesq problem as well). We can analyse the equilibrium solutions in each subspace using the results of [1] and [3].

Applying the Equivariant Hopf Theorem [13, p275, theorem 4.1] to the oscillating subspace $\mathcal{S}_1$ proves the existence of five primary branches which exist for all combinations of coefficients in the normal form. These are denoted TR

Table 2
Periodic orbits in $\mathcal{S}_1$, the form of the corresponding fixed point subspace and expressions for the signs of the real parts of the eigenvalues in $\mathcal{S}_1$ and transversely. Multiplicities are given in brackets. $f = \lambda_1 + \lambda_2 - 2\lambda_3$. TR - Travelling Rolls, TS - Travelling Squares, SR - Standing Rolls, SS - Standing Squares, AR - Alternating Rolls. Superscript r means 'the real part of'. For SR, SS and AR the underlined expressions must be negative to force the last pair of eigenvalues to have negative real parts. See [3, table 5] for further details.

Fixed Point	Solution form (A_1,A_2,B_1,B_2)	Signs of real parts of eigenvalues within $\mathcal{S}_1$	transverse to $\mathcal{S}_1$
TR	$(\mathbf{z},0,0,0)$	$0\ ^{(1)},\quad \lambda_1^r\ ^{(1)},\quad \lambda_2^r-\lambda_1^r\ ^{(2)},\quad \lambda_3^r-\lambda_1^r\ ^{(4)}$	$\mu_2 - \frac{\beta_3^r\hat{\mu}_1}{\lambda_1^r}\ ^{(4)}$
TS	$(\mathbf{z},0,\mathbf{z},0)$	$0\ ^{(2)},\quad \lambda_1^r \pm \lambda_3^r\ ^{(1)},\quad \lambda_2^r-\lambda_1^r \pm \alpha_2^r\ ^{(2)},$	$\mu_2 - \frac{2\beta_3^r\hat{\mu}_1}{\lambda_1^r+\lambda_3^r}\ ^{(4)}$
SR	$(\mathbf{z},\mathbf{z},0,0)$	$0\ ^{(2)},\quad \lambda_1^r \pm \lambda_2^r\ ^{(1)},\quad \underline{-f^r},\quad \underline{\lvert\alpha_2\rvert^2-\lvert f\rvert^2}$	$\mu_2 - \frac{(2\beta_3^r\pm\nu_2)\hat{\mu}_1}{\lambda_1^r+\lambda_2^r}\ ^{(2)}$
SS	$(\mathbf{z},\mathbf{z},\mathbf{z},\mathbf{z})$	$0\ ^{(3)},\quad \lambda_1^r-\lambda_2^r-\alpha_2^r\ ^{(2)},\quad \underline{f^r-3\alpha_2^r}$	$\mu_2 - \frac{4\beta_3^r\hat{\mu}_1}{2\lambda_3^r+\lambda_1^r+\lambda_2^r+\alpha_2^r}\ ^{(2)}$
		$f^r+4\lambda_3^r+\alpha_2^r\ ^{(1)},\quad \underline{Re\{\bar{\alpha_2}f\}-\lvert\alpha_2\rvert^2}$	$\mu_2 - \frac{(4\beta_3^r\pm2\nu_2)\hat{\mu}_1}{2\lambda_3^r+\lambda_1^r+\lambda_2^r+\alpha_2^r}\ ^{(1)}$
AR	$(\mathbf{z},\mathbf{z},i\mathbf{z},i\mathbf{z})$	$0\ ^{(3)},\quad \lambda_1^r-\lambda_2^r+\alpha_2^r\ ^{(2)},\quad \underline{f^r+3\alpha_2^r}$	$\mu_2 - \frac{4\beta_3^r\hat{\mu}_1}{2\lambda_3^r+\lambda_1^r+\lambda_2^r-\alpha_2^r}\ ^{(2)}$
		$f^r+4\lambda_3^r-\alpha_2^r\ ^{(1)},\quad \underline{-Re\{\bar{\alpha_2}f\}-\lvert\alpha_2\rvert^2}$	$\mu_2 - \frac{(4\beta_3^r\pm2\nu_2)\hat{\mu}_1}{2\lambda_3^r+\lambda_1^r+\lambda_2^r-\alpha_2^r}\ ^{(1)}$

(Travelling Rolls), TS (Travelling Squares), SR (Standing Rolls), SS (Standing Squares) and AR (Alternating Rolls). In the steady subspace there are two primary branches: DR (Diagonal Rolls) and DS (Diagonal Squares). For each point we can calculate its stability not only to perturbations within the subspace, but transversely as well. From now onwards, r will denote the modulus of a solution, as variation of the Rayleigh number is achieved by varying the bifurcation parameters $\hat{\mu}_1$ and μ_2.

In the oscillating subspace there is one more possible branch of periodic solutions, called Standing Cross Rolls (SCR). This is a solution of the form $A_1 = A_2$, $B_1 = B_2$, $|A_1| \neq |B_1|$. The existence of an SCR solution is not guaranteed by the Equivariant Hopf Theorem since its isotropy subgroup does not have a two-dimensional fixed point subspace: its existence depends on the coefficients in the normal form. It can be shown [3] that when this solution exists it is always unstable. It is still important for two reasons; it can transfer stability from one solution branch to another, and because other quasiperiodic solutions can branch from it and these quasiperiodic solutions can be stable [10].

Table 3
Fixed points in $\mathcal{S}_2$, the form of the corresponding fixed point subspace and expressions for the signs of the real parts of their eigenvalues in $\mathcal{S}_2$ and transversely. Multiplicities are given in brackets. DR - Diagonal Rolls, DS - Diagonal Squares. Note that there is a circle of equilibria in each case as the phase of $\mathbf{z}$ is arbitrary.

Fixed	Solution	Signs of real parts of eigenvalues	
Point	form (C,D)	within $\mathcal{S}_2$	transverse to $\mathcal{S}_2$
DR	$(\|\mathbf{z}\|, 0)$	$0^{\ (2)}$, $\beta_1^{\ (1)}$, $\beta_2-\beta_1^{\ (1)}$	$\hat{\mu}_1-\frac{\lambda_4^r\mu_2}{\beta_1}^{\ (8)}$
DS	$(\|\mathbf{z}\|, \|\mathbf{z}\|)$	$0^{\ (2)}$, $\beta_1+\beta_2^{\ (1)}$, $\beta_1-\beta_2^{\ (1)}$	$\hat{\mu}_1-\frac{(2\lambda_4^r\pm\alpha_3^r)\mu_2}{\beta_1+\beta_2}^{\ (4)}$

3.2 Reduction to a system of 9 real equations

The physical problem is invariant under three translation symmetries - in the x and y directions and in time. By writing the complex amplitudes as $A_1 = \tilde{A}_1 e^{i\theta_{A_1}}$, $C = \tilde{C}e^{i\theta_C}$ etc we can rewrite the equations as evolution equations for the six moduli and three combinations of the phase variables. The reduced set of equations is given in the Appendix. We define

$$\begin{aligned}\phi_1 &= \theta_{B_2} - \theta_{B_1} + \theta_C - \theta_D\\ \phi_2 &= \theta_{A_2} - \theta_{A_1} + \theta_C + \theta_D\\ \psi &= \theta_{B_1} + \theta_{B_2} - \theta_{A_1} - \theta_{A_2}\end{aligned}$$

Periodic solutions to the full system of equations are not isolated in phase space due to the continuous translation symmetries. However, these simply-periodic orbits correspond to isolated fixed points in the reduced equations (50)-(58), and periodic orbits in (50)-(58) correspond to quasiperiodic trajectories in the full equations (13)-(18); such quasiperiodic solutions will be called modulus-varying solutions. However, a fixed point of the reduced equations may correspond to a *quasiperiodic* solution of the full system: for a simply periodic solution to the full system we require $\dot{\theta}_{A_1} = \dot{\theta}_{A_2} = \dot{\theta}_{B_1} = \dot{\theta}_{B_2}$ and this may not be the case even though ψ, ϕ_1, ϕ_2 and all the moduli are constant. These are examples of relative periodic solutions for the full system: they look periodic in a suitably co-moving frame. To determine the bifurcation structure, it is much easier to follow fixed points of the reduced system (50)-(58) (in AUTO [14] for example) than it is to follow periodic orbits of the full system.

In the Boussinesq case the bifurcation structure is greatly simplified: by rescaling the amplitudes, writing $A_1 = \hat{A}_1\sqrt{\hat{\mu}_1}$, $C = \hat{C}\sqrt{\mu_2}$ etc, and dropping the carats, we can see that the real parameters $\hat{\mu}_1$, μ_2 only enter the equations in the combination $\mu_2/\hat{\mu}_1$. So all bifurcation loci will be straight lines through

the origin in the ($\hat{\mu}_1$, μ_2)-plane.

4 Boussinesq magnetoconvection

4.1 The normal form coefficients for Boussinesq magnetoconvection

The amplitude equations (13)-(18) contain a large number of undetermined constants. We will not attempt a full exploration of this parameter space but instead compute the coefficients for this particular physical problem. The idealised boundary conditions (4) allow an analytical solution for weakly nonlinear convection to be developed by using modified perturbation theory (see, for example [6]). By continuing the calculation to third order we can derive the coefficients for the cubic terms in the amplitude equations.

As usual in a modified perturbation expansion, we also expand some of the physical parameters (σ, ζ, Q and R) in powers of ϵ to provide bifurcation parameters for unfolding the behaviour of the low-order model around the onset of convection. It is easiest here to use the Rayleigh and Chandrasekhar numbers:

$$R = R_c + \epsilon r_1 + \epsilon^2 r_2 + \cdots$$
$$Q = Q_0 + \epsilon Q_1 + \epsilon^2 Q_2 + \cdots$$

r_1 and Q_1 are forced to be zero by the solvability condition imposed at second order.

Using the solvability condition at third order we can find the values of the coefficients of cubic terms as ζ varies. The values of α_1 and ν_1 cannot be found by this expansion as they are identically zero for a Boussinesq fluid. In section 5 we will explore two contrasting cases: $\alpha_1 = \nu_1$ and $\alpha_1 = -\nu_1$. By considering a weak breaking of the Boussinesq symmetry we can justify introducing the quadratic terms at the same order in ϵ as the cubic terms.

One independent check of the calculation is possible: the calculated values for λ_1 and λ_2 should (and do) agree with equation (18) in [15]; this paper gives an explicit formula (with a small printed error) for these coefficients. It is also important to relate the linear terms in the amplitude equations (those with coefficients μ_1 and μ_2) to the physical parameters r_2 and Q_2.

$$\mu_1 \equiv \hat{\mu}_1 + i\tilde{\omega} = \frac{\sigma\alpha_0^2(\zeta\beta^2 - i\omega_0)r_2 - \sigma\zeta\pi^2(\beta^2 - i\omega_0)Q_2}{2i\omega_0\beta^2[i\omega_0 - \beta^2(1+\sigma+\zeta)]} \tag{21}$$

$$\mu_2 = \frac{\sigma\zeta(2\alpha_0^2 r_2 - \pi^2\gamma^2 Q_2)}{\gamma^4\zeta + \sigma\zeta(\gamma^4 + \pi^2 Q_0) - \sigma\pi^2 Q_0} \tag{22}$$

where $\gamma^2 = 2\alpha_0^2 + \pi^2$ and $\beta^2 = \alpha_0^2 + \pi^2$. The signs of the coefficients agree with intuition - if r_2 increases we move further above the point at which convection starts and both bifurcation parameters increase, and if Q_2 increases the field inhibits the convective motion and the bifurcation parameters decrease.

To investigate the stable planforms as ζ varies, the coefficient values were interpolated between the calculated values at $\zeta = 0.1, \ldots, 0.9$.

4.2 Stable solutions in $\mathcal{S}_2$ (the steady subspace)

For all values of ζ we find $\beta_2 < \beta_1 < 0$ so both steady branches within $\mathcal{S}_2$ always bifurcate supercritically. The stable planform is Diagonal Rolls (DR), and the other primary branch, Diagonal Squares (DS), is always unstable.

4.3 Stable solutions in $\mathcal{S}_1$ (the oscillatory subspace)

The existence of stable Standing Squares for low ζ and the existence of stable Alternating Rolls and Travelling Rolls for high ζ can be deduced directly from the results of Silber and Knobloch [3].

For $0.3 \leq \zeta \leq 0.6$, though, none of the five primary periodic branches are stable. The stable attractor is a previously unnoticed doubly or triply-periodic orbit. These quasiperiodic orbits are discussed in detail in another paper [10].

The sequence of bifurcations as we increase ζ that account for the transition from stable Standing Squares (SS) to stable Alternating Rolls (AR) is summarised in table 4 and figure 3. Nearly all of this sequence of bifurcations happens within the *SCR subspace*, defined by $A_1 = A_2$ and $B_1 = B_2$, and so we could use the well-known *associated spherical system* of [16]. However, the novel part of the dynamics is not contained within this subspace. The transition from SS to AR does not involve the TR solutions which gain stability for larger ζ, so we will omit them from this discussion.

There is a Hopf bifurcation from SS when $f^r - 3\alpha_2^r = 0$ which happens when $\zeta = 0.24781$. This creates a modulus-varying quasiperiodic orbit which appears as a periodic orbit in the reduced system. The existence of this quasiperiodic solution was first noticed by Swift [16]. There is also a subcritical pitchfork bifurcation from the AR solution when $\zeta = 0.628473$. In this pitchfork bifurcation two SCR solutions are created. They are unstable as we expect.

As we increase ζ from the SS Hopf bifurcation, the periodic orbit (which remains in the SCR subspace) grows closer to the AR solution. At a critical value $\zeta = 0.45748$ there is a homoclinic connection between the stable and unstable manifolds of the AR solution. The periodic orbit splits (in a reverse 'gluing' bifurcation) into two smaller orbits which are related by the reflection symmetry m_d.

These smaller periodic orbits subsequently lose stability in a direction transverse to the SCR subspace and undergo a pitchfork bifurcation of periodic orbits at $\zeta \simeq 0.57$ to create solutions outside the SCR subspace. In the full system (13)-(18) these new solutions are triply-periodic; looking at the equations for the individual arguments of the mode amplitudes we see that $\dot{\theta}_{A_1} \neq \dot{\theta}_{A_2} \neq \dot{\theta}_{B_1} = \dot{\theta}_{B_2}$, so there are actually three independent frequencies in the system. The introduction of a third frequency is a consequence of the symmetry-breaking between the A_1 and A_2 modes which has taken place. The moduli of the amplitudes still vary periodically in the reduced system.

At $\zeta = 0.58387$ this periodic orbit (when viewed in the reduced system (50)-(58)) undergoes a reverse Hopf bifurcation and a stable "fixed point" appears in the reduced system, with $|A_1| \neq |A_2|$, $|B_1| = |B_2|$ and ψ all constant. This cannot correspond to one of the six possible simply-periodic solutions of the full system, and there are still three of the mode frequencies still different, so it is actually still a quasiperiodic solution for the full problem: $\dot{\theta}_{A_1} \neq \dot{\theta}_{A_2} \neq \dot{\theta}_{B_1} = \dot{\theta}_{B_2}$, but $\dot{\psi} = 0$, imposing the constraint

$$\dot{\psi} = \dot{\theta}_{B_1} + \dot{\theta}_{B_2} - \dot{\theta}_{A_1} - \dot{\theta}_{A_2} = 0$$

so there are only two *independent* frequencies. The corresponding planform is best described as *Drifting* Standing Cross Rolls (DSCR) and is a relative periodic orbit for the full system. Note that this doubly-periodic solution is still outside the SCR subspace, and that the moduli of the mode amplitudes are constant for this solution.

At $\zeta = 0.62607$ this DSCR solution undergoes a bifurcation back to a periodic orbit, and then at $\zeta \simeq 0.6344$ this asymmetric (in terms of A_1 and A_2) periodic orbit outside the SCR subspace has a reverse pitchfork bifurcation of periodic orbits back onto the periodic orbit contained within the SCR subspace. This orbit then disappears when it goes homoclinic to the SCR fixed points at $\zeta = 0.63876$.

This sequence of bifurcations is summarised in table 4 and in figure 3. The y-scaling of the bifurcation diagram is purely schematic since as ζ varies the interpretation of the original bifurcation parameters μ_1 and μ_2 does as well.

The existence of the stable doubly-periodic solution DSCR outside the SCR

Table 4
Summary of the stable attractors in the oscillatory subspace for $0.1 < \zeta < 0.9$. Note that for $0.628473 < \zeta < 0.63876$ there are two stable attractors.

ζ		Stable	No of indep
Between	And	Solution	Frequencies
0.1	0.24781	SS	1
0.24781	0.45748	Periodic orbit around SS	2
0.45748	0.57740	Symmetric orbit	2
0.57740	0.58387	Asymmetric orbit	3
0.58387	0.62607	'Fixed point' DSCR: $\|A_1\| \neq \|A_2\|$,$\|B_1\| = \|B_2\|$	2
0.62607	$\simeq$0.6344	Asymmetric orbit	3
$\simeq$0.6344	0.63876	Symmetric orbit	2
0.628473	0.9	AR	1

subspace is investigated in more detail in [10]. Near the bifurcation point the DSCR solution must be unstable (as the SCR solutions are always unstable) but, as happens here, it can be stabilised further away.

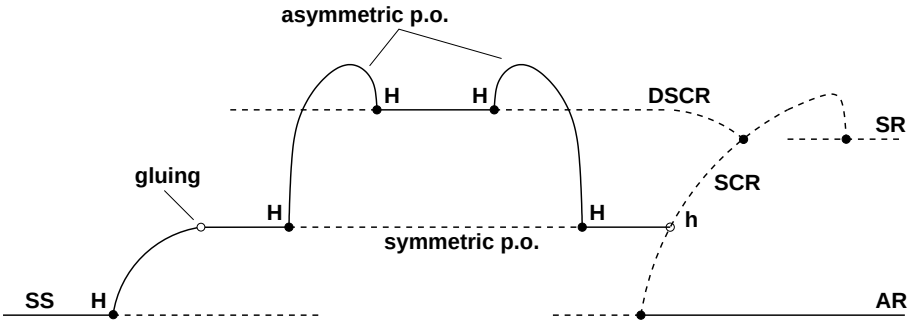

Fig. 3. Sketch bifurcation diagram showing the changes in the stable object in the subspace $\mathcal{S}_1$ as ζ increases. The DSCR solution and the asymmetric quasiperiodic orbit lie outside the SCR subspace. H - Hopf bifurcation, h - homoclinic bifurcation.

4.4 Analysis of the case $\zeta = 0.1$

For $\zeta = 0.1$, all branches in $\mathcal{S}_1$ or $\mathcal{S}_2$ bifurcate supercritically (into $\hat{\mu}_1 > 0$ or $\mu_2 > 0$ respectively). Since all bifurcation loci are straight lines through the origin, we will use the angle $\theta = \tan^{-1}(\mu_2/\hat{\mu}_1)$ as the bifurcation parameter. For the rest of the paper we will drop the carat on $\hat{\mu}_1$. Standing Squares (SS) are the only stable solution in $\mathcal{S}_1$ and Diagonal Rolls (DR) are stable in $\mathcal{S}_2$. The SS solution is stable against transverse perturbations when all its transverse eigenvalues are negative which requires

$$\mu_2 - \frac{(4\beta_3^r - 2\nu_2)\mu_1}{2\lambda_3^r + \lambda_1^r + \lambda_2^r + \alpha_2^r} < 0 \tag{23}$$

for $\zeta = 0.1$ this condition gives $-\pi/2 < \theta < -1.4466$. Similarly, DR are stable against transverse perturbations when

$$\mu_1 - \frac{\lambda_4^r \mu_2}{\beta_1} < 0 \tag{24}$$

which for $\zeta = 0.1$ requires $\pi > \theta > 2.4137$.

Subsections 4.4.1–4.4.5 below follow a path of increasing θ (anticlockwise) around the origin in the (μ_1,μ_2)-plane, starting in the lower-left quadrant. The bifurcation structure was computed numerically using AUTO [14] and confirmed by the analytic results presented below.

4.4.1 Bifurcations from Standing Squares

As we cross the line $\theta = -1.4466$, one Floquet multiplier of the SS periodic orbit crosses the unit circle at $+1$ and there is a pitchfork bifurcation of the periodic orbit. Stable solutions representing standing squares with a constant amount of diagonal squares superimposed are created. Looking at the linearised equations for perturbations to the SS solution we can determine the eigenvector corresponding to the bifurcating solution. When C and D are small we have (from (13)-(18)), splitting C and D into their real and imaginary parts:

$$\begin{pmatrix} \dot{C}_r \\ \dot{D}_r \\ \dot{C}_i \\ \dot{D}_i \end{pmatrix} = \begin{pmatrix} \mu_2 + 4\beta_3^r r_{SS}^2 & 2\nu_2 r_{SS}^2 & 0 & 0 \\ 2\nu_2 r_{SS}^2 & \mu_2 + 4\beta_3^r r_{SS}^2 & 0 & 0 \\ 0 & 0 & \mu_2 + 4\beta_3^r r_{SS}^2 & 0 \\ 0 & 0 & 0 & \mu_2 + 4\beta_3^r r_{SS}^2 \end{pmatrix} \begin{pmatrix} C_r \\ D_r \\ C_i \\ D_i \end{pmatrix} \tag{25}$$

This matrix has eigenvalues $\mu_2 + 4\beta_3^r r_{SS}^2 \pm 2\nu_2 r_{SS}^2$ and $\mu_2 + 4\beta_3^r r_{SS}^2$ (twice). The eigenvector corresponding to the first eigenvalue to become zero as θ increases is $(1, -1, 0, 0)^T$, i.e. perturbations with $C_r = -D_r$ in linear theory. The bifurcating solutions are denoted *Standing Squares plus Diagonal Squares* (SS+DS). In the modulus and argument reduced system this SS+DS solution is of the form $A_{1,2}^2 = B_{1,2}^2 = r_A^2$, $C^2 = D^2 = r_C^2$, $\phi_1 = \pi, \phi_2 = \pi, \psi = 0$. These amplitudes can be found analytically:

$$r_A^2 = \frac{\mu_1(\beta_1+\beta_2) - \mu_2(2\lambda_4^r - \alpha_3^r)}{(4\beta_3^r - 2\nu_2)(2\lambda_4^r - \alpha_3^r) - (\lambda_1^r + \lambda_2^r + 2\lambda_3^r + \alpha_2^r)(\beta_1+\beta_2)}$$

$$r_C^2 = \frac{\mu_2(\lambda_1^r + \lambda_2^r + 2\lambda_3^r + \alpha_2^r) - \mu_1(4\beta_3^r - 2\nu_2)}{(4\beta_3^r - 2\nu_2)(2\lambda_4^r - \alpha_3^r) - (\lambda_1^r + \lambda_2^r + 2\lambda_3^r + \alpha_2^r)(\beta_1+\beta_2)}$$

Note that this solution SS+DS is in the subspace $\{\phi_1 = \pi, \phi_2 = \pi, \psi = 0\}$, not the subspace $\{\phi_1 = 0, \phi_2 = 0, \psi = 0\}$. Thus it does not have the full symmetry group D_4, but only reflections in diagonal lines m_d and $m_{d'}$ which generate a group $\mathbb{Z}_2^2$. However, it also other symmetries which will be discussed in section 4.5.1. This SS+DS solution is stable for $-1.4466 < \theta < 1.1534$.

4.4.2 Bifurcations from Standing Squares + Diagonal Squares

Two distinct types of bifurcation from SS+DS take place. One is to solutions denoted *type 1* and *type 2* which break the equality of the amplitudes of the oscillatory modes, and one is to *type 3* solutions which breaks the equality of the steady modes. We will analyse each in terms of the marginal modes, and then in section 4.5.1 this will be set in a more general symmetry-breaking context. By using the reduced system we can look for zero eigenvalues of the Jacobian matrix rather than marginal Floquet multipliers.

Bifurcations from SS+DS to type 1 and 2 solutions

Numerical continuation of the SS+DS solution indicates that two new solution branches bifurcate from SS+DS at the same point. These two solutions can be distinguished by their symmetries: type 1 solutions are invariant under the reflection m_d in the line $y = x$ and type 2 solutions have no simple reflection symmetries. This can be explained by perturbing around the SS+DS solution; The simultaneous existence of two independent modes with zero eigenvalues can be shown by perturbing about the original fixed point of the reduced system (50)-(58). Write

$$\begin{aligned} A_1 &= r_A + u \qquad B_1 = r_A + v \qquad \phi_1 = \pi + \hat{\phi}_1 \qquad C = D = r_C \\ A_2 &= r_A - u \qquad B_2 = r_A - v \qquad \phi_2 = \pi + \hat{\phi}_2 \qquad \psi = \hat{\psi} \end{aligned} \tag{26}$$

and say $\hat{\phi}_1, \hat{\phi}_2$ and $\hat{\psi}$ are all small (they are identically zero for the SS+DS solution). Then, linearising the equations for $u, v, \hat{\phi}_1, \hat{\phi}_2$ and $\hat{\psi}$ (dropping the hats) we find

$$\dot{u} = u\Big[\mu_1 + (3\lambda_1^r - \lambda_2^r + 2\lambda_3^r - \alpha_2^r)r_A^2 + (2\lambda_4^r + \alpha_3^r)r_C^2\Big] + \alpha_3^i r_A r_C^2 \phi_2$$

$$\equiv f(u,\phi_2) \tag{27}$$

$$\dot{\phi_2} = 4u\Big[(2\beta_3^i - \lambda_1^i + \lambda_2^i + \alpha_2^i)r_A - \alpha_3^i\frac{r_C^2}{r_A}\Big] + 2\phi_2(\alpha_3^r r_C^2 + \nu_2 r_A^2)$$

$$\equiv g(u,\phi_2) \tag{28}$$

$$\dot{v} = f(v,\phi_1) \tag{29}$$

$$\dot{\phi_1} = g(v,\phi_1) \tag{30}$$

$$\dot{\psi} = -4\alpha_2^r r_A^2 \psi \tag{31}$$

The ψ equation decouples, and there is a double real zero eigenvalue of the linearised system at the bifurcation point. By constructing the centre manifold, or using symmetry arguments (see section 4.5.2) we can show that there are two bifurcating solution branches.

To find the bifurcation point we substitute in for r_A and r_C and solve the resulting quadratic in μ_2 (for a fixed value of μ_1). For $\zeta = 0.1$ there are two real roots at $\theta = 1.1534$ and $\theta = 1.3097$; there are two double-zero bifurcation points for $\zeta = 0.1$.

At $\theta = 1.1534$, we find that both branches bifurcate supercritically, type 1 solutions are unstable, and type 2 solutions are stable. The inequality of solution amplitudes means that the solution modes do not oscillate at equal frequencies $\dot{\theta}_i$ (the normal form symmetry h has been broken). This small discrepancy in frequencies leads to the solutions appearing to 'drift' in physical space. This drift is examined in more detail in section 4.5.2. Figure 9(a) below shows the instantaneous planform of a type 1 solution, and figure 9(b) shows a type 2 solution.

At the second interaction point $\theta = 1.3097$ both branches are supercritical. However, neither branch is stable because the SS+DS solution has already lost stability at the earlier bifurcation. Type 2 solutions remain stable in the region $1.1534 < \theta < 1.3121$. At $\theta = 1.3121$ there is a bifurcation to a totally mixed mode (MM) solution of the form $\{A_1 \neq A_2, B_1 \neq B_2, C \neq D, \phi_1 \neq \pi, \phi_2 \neq \pi, \psi \neq 0\}$. This joins another branch at $\theta = 1.3133$ which is of the form $\{A_1 = B_2, A_2 = B_1, C \neq D, \phi_1 = -\phi_2 \neq \pi, \psi = 0\}$ which is denoted *type 4*. This type 4 branch undergoes a secondary Hopf bifurcation at $\theta = 1.3215$ to a modulus-varying solution. This is all summarised in figure 4.

Bifurcation from SS+DS $\rightarrow$ *SS+*$\{C \neq D\}$ (type 3)

A completely different bifurcation from SS+DS is to break the equality of the C and D amplitudes. From perturbing around the SS+DS solution we find that the bifurcation occurs at

$$\tan\theta = \frac{4\left[\beta_3^r(\beta_1-\beta_2)-\nu_2\beta_1\right]}{(\beta_1-\beta_2)(\lambda_1^r+\lambda_2^r+2\lambda_3^r+\alpha_2^r)-2\nu_2(2\lambda_4^r-\alpha_3^r)} \tag{32}$$

For $\zeta = 0.1$ this gives a value of $\theta = 1.2610$. We can solve the reduced amplitude equations (50)-(58) directly to find the amplitudes of the modes in the type 3 solution:

$$A_{1,2}^2 = B_{1,2}^2 = r_A^2 = \frac{(\mu_1\beta_1-\lambda_4^r\mu_2)(\beta_1-\beta_2)}{(4\lambda_4^r\beta_3^r-X\beta_1)(\beta_1-\beta_2)-2\nu_2\alpha_3^r\beta_1} \tag{33}$$

$$C^2 = \frac{p+(p^2-4q^2)^{1/2}}{2} \tag{34}$$

$$D^2 = \frac{p-(p^2-4q^2)^{1/2}}{2} \tag{35}$$

where p and q are defined as

$$p = C^2+D^2 = \frac{(\beta_2-\beta_1)(4\mu_1\beta_3^r-X\mu_2)+2\nu_2\alpha_3^r\mu_2}{(4\lambda_4^r\beta_3^r-X\beta_1)(\beta_1-\beta_2)-2\nu_2\alpha_3^r\beta_1} \tag{36}$$

$$q = CD = \frac{2\nu_2A^2}{\beta_2-\beta_1} \tag{37}$$

and $X = \lambda_1^r+\lambda_2^r+2\lambda_3^r+\alpha_2^r$.

4.4.3 Bifurcation from type 3 to type 4 solutions

Can a type 3 solution become unstable to perturbations in the A and B modes in the same way that SS+DS can? Going back to the perturbation equations (27)-(30) the equations for u and v are unchanged, except for writing $C = r_C$ and $D = r_D$ which are not assumed to be equal. However, extra terms appear in equations (30) and (28) for $\hat{\phi_1} = \phi_1 - \pi$ and $\hat{\phi_2} = \phi_2 - \pi$, coupling them together (below we have dropped the hats again).

$$\dot{\phi_2} = \cdots - \nu_2 r_A^2\Big(\frac{r_C}{r_D}-\frac{r_D}{r_C}\Big)\phi_1 + \nu_2 r_A^2\Big(\frac{r_C}{r_D}+\frac{r_D}{r_C}\Big)\phi_2$$
$$\dot{\phi_1} = \cdots - \nu_2 r_A^2\Big(\frac{r_C}{r_D}-\frac{r_D}{r_C}\Big)\phi_2 + \nu_2 r_A^2\Big(\frac{r_C}{r_D}+\frac{r_D}{r_C}\Big)\phi_1$$

So we do not now have the double zero eigenvalue situation that we had before and there is only one solution branch. This is labelled the *type 4* solution, as it differs from the type 1 solution in having $|C|$ and $|D|$ unequal. They do, however, have identical spatial reflection symmetries. This bifurcation from type 3 to type 4 occurs at $\theta = 1.2612$ for $\zeta = 0.1$. The type 4 branch is stable for $1.3133 < \theta < 1.3215$ (see figure 4). The Hopf bifurcation from type

4 solutions produces a quasiperiodic orbit which is represented as a periodic orbit in the reduced system, and hence is labelled $PO1$ on figure 4.

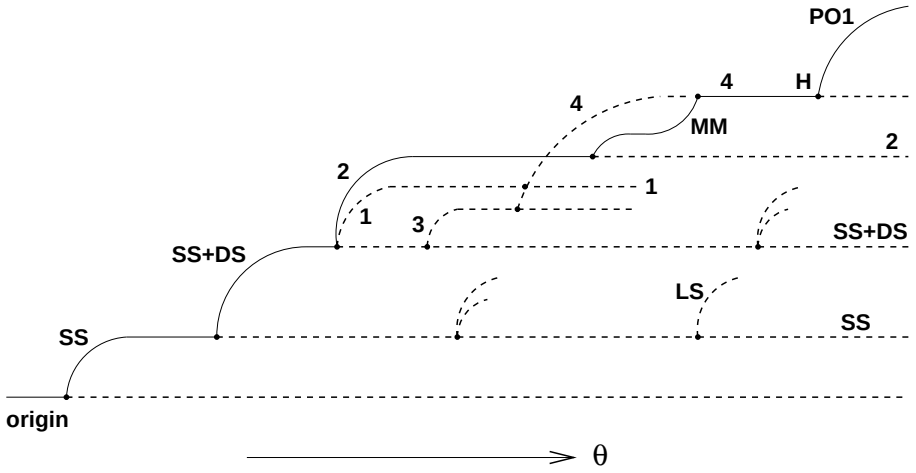

Fig. 4. Part 1 of the bifurcation diagram obtained by travelling anticlockwise around the origin in the (μ_1, μ_2)-plane. Simply-periodic orbits in the full system are represented as fixed points. Type 1, 2, 3 and 4 solutions are labelled as such. *MM* refers to the mixed mode solution. LS - oscillating 'Large Squares' solution. H - Hopf bifurcation (in the reduced system). Note the transcritical bifurcation between type 1 and type 4 solutions. The *MM* branch and subsequent bifurcations were carefully determined using AUTO.

There are many other bifurcations involving fixed points in this system, including homoclinic ones. However, they all involve unstable fixed points and periodic orbits so we will disregard them. The bifurcation diagram shows those fixed points which bifurcate from the SS+DS solution, and is a complete investigation of their behaviour. There are also solutions which bifurcate from each of the other 4 primary solution branches (guaranteed by the Equivariant Hopf Theorem) in the oscillatory invariant subspace (these are TR, TS, SR and AR). These all follow bifurcation diagrams similar to that given for SS, but all the solution branches are unstable and so they have no physical relevance.

4.4.4 Stable modulus-varying solutions

The secondary Hopf bifurcation from type 4 solutions takes place at $\theta = 1.3215$ and this periodic orbit (in the reduced system) is stable in the region $1.3215 < \theta < 1.3622$. This periodic orbit preserves the symmetry of the type 4 fixed point; points on the orbit satisfy $\{A_1 = B_1, A_2 = B_2, C \neq D, \phi_1 = \phi_2 \neq 0, \psi = 0\}$. The periodic orbit undergoes another Hopf bifurcation to a 2-torus at $\theta = 1.3622$. For $1.3622 < \theta < 1.3744$ this quasiperiodic orbit is stable; for higher values of θ numerical results indicate the breakup of the 2-torus and the existence of a strange attractor (see figure 5).

This strange attractor is stable up to $\theta = 1.3760$ when a new stable periodic orbit *PO2* appears. This new periodic orbit has the same symmetries as the previous one; points on it satisfy $\{A_1 = B_1, A_2 = B_2, C \neq D, \phi_1 = \phi_2 \neq 0, \psi = 0\}$. Numerical results show that *PO2* is a different orbit to the earlier one, and the projection of *PO2* onto the $(|A_1|, |A_2|)$-plane is a figure-of-eight shape, not a simple closed curve as for the first periodic orbit.

After a symmetry-breaking bifurcation, this periodic orbit undergoes a period-doubling bifurcation at $\theta = 1.3925$, and then a period-undoubling bifurcation at $\theta = 1.3954$. It is stable in the interval $1.3954 < \theta < 1.3957$ before disappearing in a saddle-node bifurcation of periodic orbits. For higher values of θ trajectories are attracted to a different strange attractor (SA-2 in figure 5).

In the interval $1.3954 < \theta < 1.4514$ there is a complex sequence of transitions between different strange attractors and stable periodic orbits. There is often more than one stable object at a fixed parameter value.

For $1.4514 < \theta < 2.2270$ trajectories are attracted to a new strange attractor which turns into a 2-torus for $2.2270 < \theta < 2.4137$. This torus is created directly in the bifurcation when the steady solution DR becomes unstable to perturbations in the A_i and B_i modes, transverse to the steady invariant subspace.

4.4.5 The Hopf bifurcation from Diagonal Rolls (DR)

The Hopf bifurcation from DR does not result in a solution combining DR with one of the five primary branches created in a $D_4 \ltimes T^2$-symmetric Hopf bifurcation because of the cubic terms with coefficient ν_2 in equations (17) and (18). When the oscillatory modes are excited, the second steady mode must also be non-zero; hence the dynamics within the subspace $\mathcal{S}_2$ are altered as well as those in transverse directions and the Hopf bifurcation creates a 2-torus in the reduced system, ie a triply-periodic solution. Scaling arguments show that if the DR solution is given by $|C|^2 = -\mu_2/\beta_1$, $D = 0$ then, near the bifurcation point when A_i and B_i are $\mathcal{O}(\epsilon)$, D is $\mathcal{O}(\epsilon^2)$. This is confirmed by numerical integrations.

A summary sketch bifurcation diagram completing the circuit anticlockwise around the origin is given in figure 5. Bifurcations involving strange attractors are conjectural but all others were determined carefully using AUTO. It is entirely possible that other stable strange attractors or periodic solutions exist in this region of the (μ_1,μ_2)-plane.

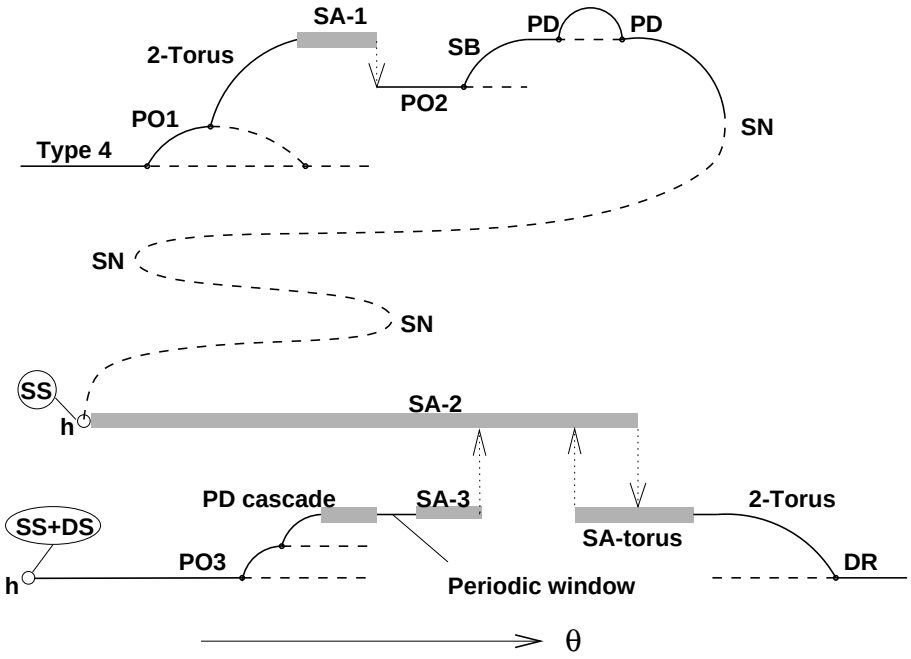

Fig. 5. Completion of the bifurcation diagram in figure 4 travelling anticlockwise around the origin in the (μ_1, μ_2)-plane. Nomenclatures refer to the appearance of orbits in the reduced system of equations. PD - Period Doubling bifurcation. SN - Saddle-Node bifurcation. SB - Symmetry-breaking bifurcation of a periodic orbit. h - homoclinic bifurcation (with the fixed point involved shown in a circle). *SA* indicates a strange attractor. Four distinct strange attractors were found numerically. Arrows show where numerical integrations close to an attractor jumped to a different attractor as the basin of attraction shrank. The bifurcation which destroys the attractor has not been investigated. Within the strange attractor *SA-3* there are windows where stable periodic orbits exist.

4.5 Bifurcation analysis in terms of spatial symmetries.

By studying the group theoretic aspects of the problem we can obtain classifications of all possible bifurcations; these heavy restrictions provide important verification of numerical and experimental results [17,18]. A very general framework for the investigation of symmetry-breaking bifurcations from non-isolated periodic orbits with spatio-temporal symmetries has been recently developed by Wulff, Lamb and Melbourne [19,20]. Due to several simplifications here: the spatiotemporal symmetry element h commutes with all purely spatial symmetries, so $k = 1$ in the notation of [19], the use of the reduced system, and the need only to consider spatial symmetry breaking, we are able to present the results in a much less technical way.

Finite groups have a finite number of irreducible matrix representations (*irreps*). For each irrep the matrix representing each group element is unique up to conjugacy. The traces of such matrices are invariant under such conjugacy operations, and so these traces uniquely specify an irrep. Furthermore this

invariance property shows that matrices representing elements in the same conjugacy class of the group must have the same character in any irrep. This information (and more, see for example [21]) enables us to construct the *character table* for $\mathcal{G}$ which classifies the possible symmetry-breaking bifurcations from a solution with symmetry $\mathcal{G}$.

4.5.1 Classification of bifurcations from Standing Squares

As we will not consider bifurcations which alter the spatial periodicity of the solutions, we will ignore the pure spatial translations which form the T^2 part of the symmetry group of the problem. The spatio-temporal symmetry h of a periodic solution is preserved by any perturbation which involves only steady modes, so all bifurcating solutions from Standing Squares considered in this section must preserve h. We consider bifurcations as being from a fixed point of the reduced system (50)-(58) so we can analyse bifurcations in terms of eigenvalues and eigenvectors.

The spatial symmetries of Standing Squares form the group D_4 generated by a y-axis reflection m_y and a reflection m_d in the line $x = y$. The rotation of $\pi/2$ anticlockwise is denoted $\rho = m_y \circ m_d$. $m_{d'} = \rho \circ m_d \circ \rho^3$ is a reflection in the line $y = -x$. The existence of the Boussinesq symmetry (19) results in a further purely spatial symmetry of Standing Squares: $\tilde{\tau} : (x, y, z, t) \to (x + \pi/\alpha, y + \pi/\alpha, 1 - z, t)$, i.e. reflection in the mid-plane of the fluid followed by a translation of half a wavelength in the x and y directions. The full spatial symmetry group of Standing Squares is $?_{SS} = D_4 \times \{Id, \tilde{\tau}\}$. The group $?_{SS}$ has 10 conjugacy classes, so (by the orthogonality properties of characters) it must have 10 irreps. The character table for $?_{SS}$ is given in Table 5.

At a bifurcation point, the dynamics are determined by the behaviour on the centre manifold. The action of $?_{SS}$ on the mode amplitudes is determined exactly as before, in section 3. This, in turn, means that $?_{SS}$ acts on the tangent space to the centre manifold. This action of $?_{SS}$ will generically be irreducible and so must correspond to one of the irreps listed in table 5. If there is only one eigenvector, each symmetry will act as ± 1 on the eigenvector and we can associate a unique one-dimensional irrep with the bifurcation. The new state produced in the bifurcation will have a symmetry group consisting of all the symmetries in $?_{SS}$ which acted trivially (i.e. as $+1$) on the eigenvector. This symmetry group is (by definition) then the isotropy subgroup of the new (bifurcated) solution.

If there are two independent eigenvectors then the action of the symmetries on the marginal modes can be represented by a set of real 2×2 matrices. The evolution equations for the marginal modes must be equivariant with respect to these matrices; this restricts the form of these evolution equations. The

Table 5
The Character Table for Γ_{SS}. The irreps are listed in the natural order given by the induction from the character tables of D_4 and $\{Id, \tilde{\tau}\}$. Writing $\tilde{\tau} \circ \rho$ denotes the group element given by their composition.

Irrep	Conjugacy Classes									
	Id	ρ	ρ^2	m_x	m_d	$\tilde{\tau}$	$\tilde{\tau} \circ \rho$	$\tilde{\tau} \circ \rho^2$	$\tilde{\tau} \circ m_x$	$\tilde{\tau} \circ m_d$
		ρ^3		m_y	$m_{d'}$		$\tilde{\tau} \circ \rho^3$		$\tilde{\tau} \circ m_y$	$\tilde{\tau} \circ m_{d'}$
χ_1	1	1	1	1	1	1	1	1	1	1
χ_2	1	1	1	-1	-1	1	1	1	-1	-1
χ_3	1	1	1	1	1	-1	-1	-1	-1	-1
χ_4	1	1	1	-1	-1	-1	-1	-1	1	1
χ_5	2	0	-2	0	0	2	0	-2	0	0
χ_6	2	0	-2	0	0	-2	0	2	0	0
χ_7	1	-1	1	1	-1	1	-1	1	1	-1
χ_8	1	-1	1	-1	1	1	-1	1	-1	1
χ_9	1	-1	1	1	-1	-1	1	-1	-1	1
χ_{10}	1	-1	1	-1	1	-1	1	-1	1	-1

absence of an irrep of dimension three or higher for this problem shows that symmetry cannot force three simultaneously zero eigenvalues here. In all cases we then apply the Equivariant Branching Lemma [13, page 82, theorem 3.3]: by the Equivariant Branching Lemma, we are guaranteed bifurcating solutions with isotropy subgroups which have one-dimensional fixed point subspaces. To find which subgroups of $?_{SS}$ are isotropy subgroups with one-dimensional fixed point subspaces it is essential to have first identified the irrep.

Using this general theory we can analyse the three possibilities for bifurcations from Standing Squares. The marginal eigenvectors are elements of a four-dimensional real vector space corresponding to perturbations in the real and imaginary parts of C and D (see equation (25)).

(a) Eigenvector $(1, 1, 0, 0)$, $u = C_r + D_r$ is the marginal mode so the centre manifold is one-dimensional.

(b) Eigenvector $(1, -1, 0, 0)$, $u = C_r - D_r$ is the marginal mode so the centre manifold is one-dimensional.

(c) Eigenvectors $(0, 0, 1, 0)$ and $(0, 0, 0, 1)$, $u = C_i$ and $v = D_i$ are simultaneously marginal modes so the centre manifold is two-dimensional.

In case (a) the elements of $?_{SS}$ which act as $+1$ are exactly those in D_4. Thus

the bifurcation breaks the $\tilde{\tau}$ symmetry of SS and corresponds to irrep χ_3. The existence of group elements which act as -1 on the 1D centre manifold means that the bifurcation is a pitchfork, and the dynamics are governed by an equation of the form $\dot{u} = \kappa u + bu^3$.

In case (b) the elements of $?_{SS}$ which act as $+1$ are $\{Id, m_d, m_{d'}, \rho^2, \tilde{\tau} \circ \rho, \tilde{\tau} \circ \rho^3, \tilde{\tau} \circ m_x, \tilde{\tau} \circ m_y\}$. These elements form a group isomorphic to D_4, but distinct from it. We shall denote this group $\tilde{D}_4$. The corresponding irrep is χ_{10}, and again the bifurcation is a pitchfork, with dynamics on the centre manifold given by the pitchfork normal form.

Case (c) must correspond to one of the two two-dimensional irreps of $?_{SS}$. Looking at the action of the group elements we find that because $\tilde{\tau} : (u, v) \to (-u, -v)$, it must be irrep χ_6. The two one-dimensional fixed point subspaces are $(u, 0)$ and (u, u). These have symmetry groups $\{Id, m_d, \tilde{\tau} \circ m_{d'}, \tilde{\tau} \circ \rho^2\}$ and $\{Id, m_x, \tilde{\tau} \circ m_y, \tilde{\tau} \circ \rho^2\}$ respectively. Both these groups are isomorphic to $\mathbb{Z}_2^2$. On the centre manifold, the equations for $\dot{u}$ and $\dot{v}$

$$\begin{pmatrix} \dot{u} \\ \dot{v} \end{pmatrix} = \begin{pmatrix} f(u, v) \\ g(u, v) \end{pmatrix} \tag{38}$$

must be equivariant with respect to the action of the symmetries, i.e.

$$R_g \begin{pmatrix} f(u, v) \\ g(u, v) \end{pmatrix} = \begin{pmatrix} f(R_g(u, v)) \\ g(R_g(u, v)) \end{pmatrix} \tag{39}$$

where R_g is a 2×2 matrix representing a group element. The centre manifold equations must therefore look like

$$\dot{u} = u\Big[\kappa + av^2 + b(u^2 + v^2)\Big] \tag{40}$$

$$\dot{v} = v\Big[\kappa + au^2 + b(u^2 + v^2)\Big] \tag{41}$$

when truncated at third order. In theory we can perform the centre manifold reduction and determine the real coefficients κ, a and b in terms of the normal form coefficients. The planforms of the two solution branches $(u, 0)$ and (u, u) are shown in figure 8.

In this particular problem, because the coefficient $\nu_2 < 0$, we find that case (b), the bifurcation to SS+DS solutions, occurs for the lowest value of the parameter θ. If case (a) had occurred for a lower value of θ, we would stay in the subspace with $\phi_1 = \phi_2 = \psi = 0$ which Proctor and Matthews [8] call $\mathcal{PR}$

and we would observe an oscillating version of their "Large Squares" solution. The behaviour here is very different because it corresponds to a different irrep of the symmetry group of the pattern. Figures 6–8 show instantaneous views of solutions to (13) - (18) showing the different patterns produced in these bifurcations. Each figure shows contours of constant vertical fluid velocity at the mid-plane of the fluid layer. Solid contours represent upwards flow, dashed contours represent downwards flow.

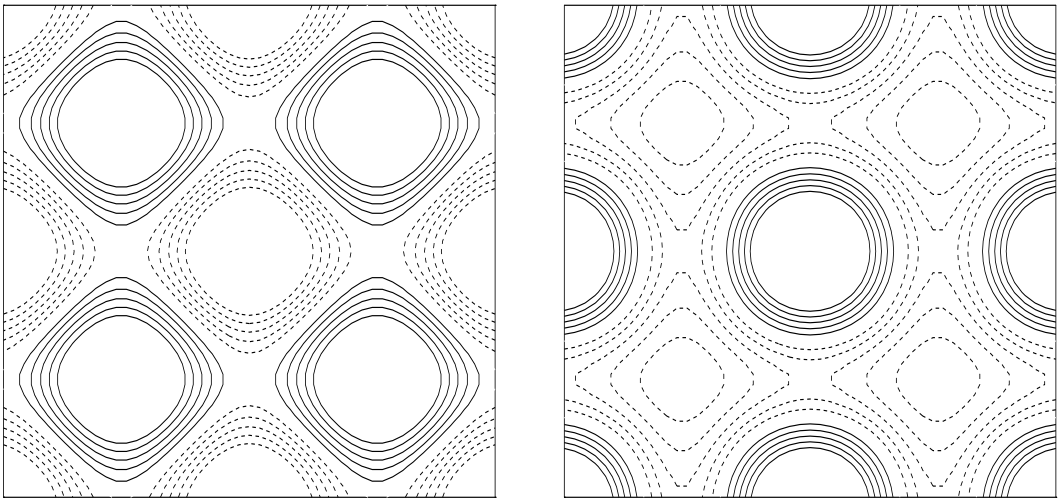

(a) (b)

Fig. 6. Instantaneous views of (a) Standing Squares, and (b) Oscillating 'Large Squares' created in a bifurcation corresponding to a marginal mode $u = C_r + D_r$. In (b) the solution has a spatial symmetry group D_4 - it has lost the symmetry $\tilde{\tau}$. Both solutions have symmetry h, but this cannot be detected from an instantaneous view.

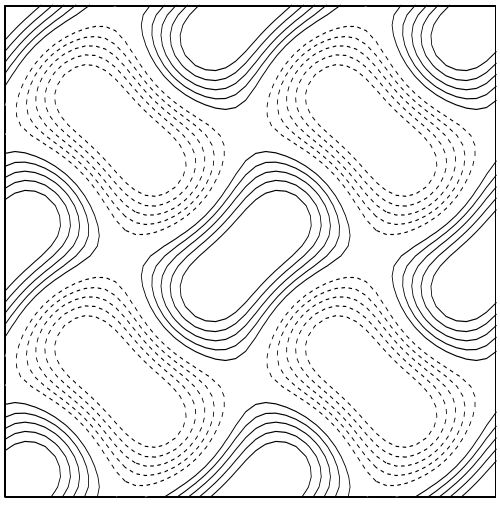

Fig. 7. An instantaneous view of the SS+DS solution corresponding to the choice of $u = C_r - D_r$ as the marginal mode. This is the case that occurs first for $\zeta = 0.1$ and gives a solution with spatial symmetry group $\tilde{D}_4$ and spatio-temporal symmetry h.

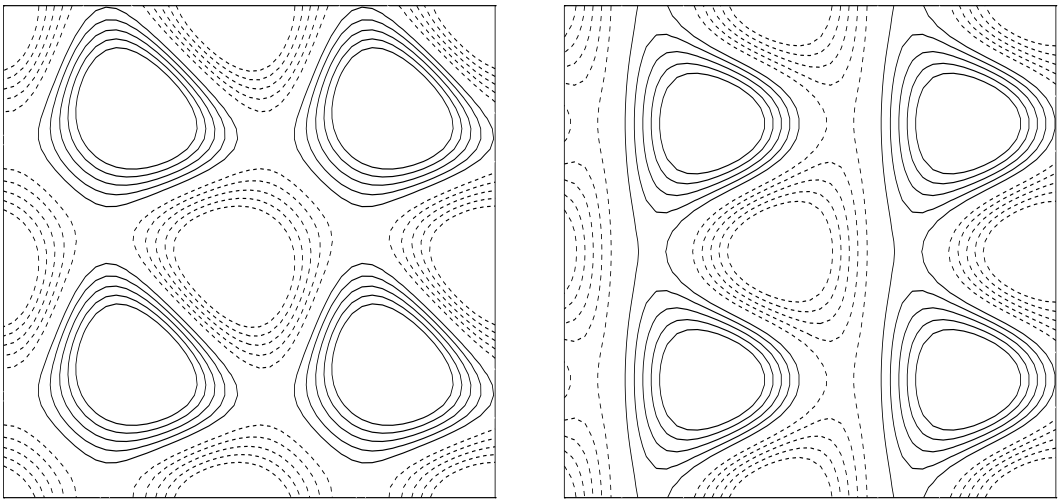

(a) (b)

Fig. 8. Instantaneous views of the two bifurcating planforms from the double zero bifurcation: (a) SS+DR (Diagonal Roll) branch corresponding to $v = C_i$, (b) SS+DS (Diagonal Squares) II branch with marginal mode $v = C_i = w = D_i$. Both have a spatial symmetry group isomorphic to $\mathbb{Z}_2^2$ and in addition preserve the symmetry h.

4.5.2 Classification of bifurcations from SS+DS

Exactly as for the bifurcations from SS, we can look at bifurcations from SS+DS in terms of the irreps of the symmetry group of the SS+DS solution: $?_{SS+DS} = \tilde{D}_4 \times \{Id, h\}$ (h is the spatiotemporal symmetry defined in section 3). This group has 10 conjugacy classes, and hence 10 irreps. The character table of $?_{SS+DS}$ is the same as that of $?_{SS}$ as the two groups are isomorphic.

As before we can identify which irrep is relevant to a bifurcation by looking at the action of each symmetry element on the eigenvectors corresponding to the zero eigenvalues at the bifurcation point.

For the first bifurcation there are two marginal modes (see equations (27)-(30)): $u = (A_1 - A_2)/2$ and $v = (B_1 - B_2)/2$. The spatio-temporal symmetry h is broken, so the relevant irrep is χ^6. There will be guaranteed bifurcating solutions of the form $(u, v) = (u, 0)$ and (u, u). The solution $(u, 0)$ has symmetry group $\{Id, m_d\}$ (type 1 - see figure 9(a)) and the solution (u, u) has symmetry group $\{Id, \tilde{\tau} \circ m_y\}$ (type 2 - see figure 9(b)). Both these groups are isomorphic to $\mathbb{Z}_2$.

By the same argument as in case (c) in the previous section, the centre manifold equations for the marginal modes look like (40) and (41) in this case as well. From the form of the bifurcation diagram (which we have already determined through AUTO) the coefficients must satisfy $a + 2b < 0 < a$.

For the bifurcation to SS+{C≠D} (type 3) solutions, the marginal mode is

Table 6
The character table for $\Gamma_{SS+DS} = \tilde{D}_4 \times \{Id, h\}$.

Irrep	Conjugacy classes									
	Id	$\tilde{\tau} \circ \rho$	ρ^2	m_d	$\tilde{\tau} \circ m_x$	h	$h \circ \rho^2$	$h \circ m_d$	$h \circ \tilde{\tau} \circ \rho$	$h \circ \tilde{\tau} \circ m_x$
		$\tilde{\tau} \circ \rho^3$		$m_{d'}$	$\tilde{\tau} \circ m_y$			$h \circ m_{d'}$	$h \circ \tilde{\tau} \circ \rho^3$	$h \circ \tilde{\tau} \circ m_y$
χ^1	1	1	1	1	1	1	1	1	1	1
χ^2	1	1	1	-1	-1	1	1	1	-1	-1
χ^3	1	1	1	1	1	-1	-1	-1	-1	-1
χ^4	1	1	1	-1	-1	-1	-1	-1	1	1
χ^5	2	0	-2	0	0	2	0	-2	0	0
χ^6	2	0	-2	0	0	-2	0	2	0	0
χ^7	1	-1	1	1	-1	1	-1	1	1	-1
χ^8	1	-1	1	-1	1	1	-1	1	-1	1
χ^9	1	-1	1	1	-1	-1	1	-1	-1	1
χ^{10}	1	-1	1	-1	1	-1	1	-1	1	-1

$u = C_r - D_r$. The symmetries that act as $+1$ on u are $\{Id, m_d, m_{d'}, \rho^2, h\}$, and this bifurcation corresponds to irrep χ^7 (as this bifurcation involves only steady modes in the marginal eigenvectors it must preserve the spatio-temporal symmetry h).

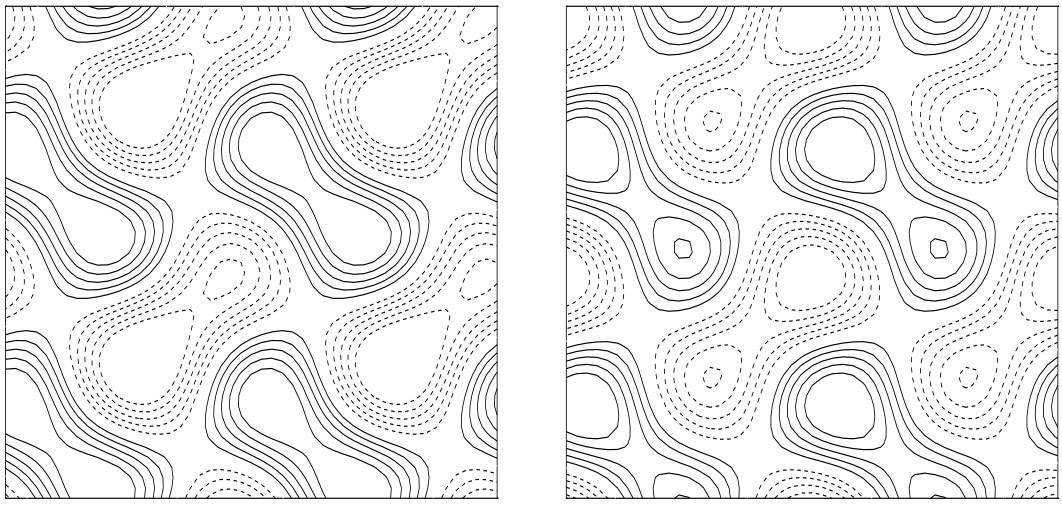

(a) (b)

Fig. 9. Instantaneous views of (a) the type 1 solution planform and (b) the type 2 planform. The type 1 solution has symmetry group $\mathbb{Z}_2 = \{Id, m_d\}$ and drifts slowly along the $y = x$ diagonal as well as executing a vertical oscillation. Similarly, the type 2 solution has a symmetry group $\mathbb{Z}_2 = \{Id, \tilde{\tau} \circ m_y\}$ and drifts slowly in the y-direction.

It is important to note that drifting solutions break the symmetry ρ^2 - the direction of drift cannot be invariant under a half-turn rotation. From table 6 we can see that, for this problem, this can only happen when the symmetries act as χ^5 or χ^6, forcing a double-zero eigenvalue. This illustrates to what a great extent possible bifurcations are constrained by symmetry.

4.5.3 Summary of the Boussinesq behaviour for $\zeta = 0.1$

A summary of the behaviour for $\zeta = 0.1$, sketching the regions of stability of each solution in the (μ_1, μ_2)-plane, is shown in figure 10(a).

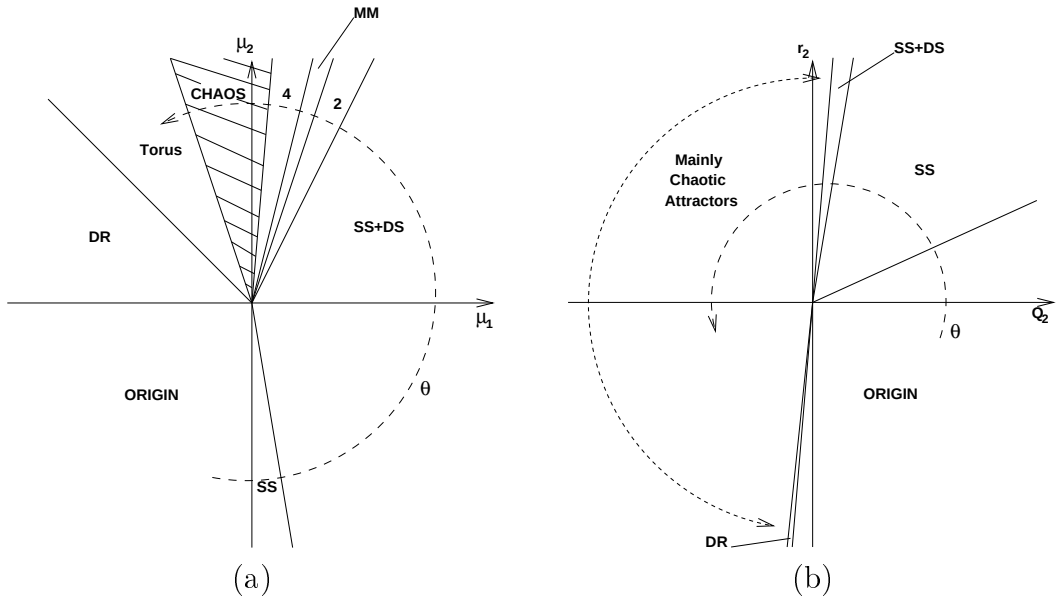

Fig. 10. Regions of stability of different solutions for the Boussinesq problem at $\zeta = 0.1$ in (a) the (μ_1, μ_2)-plane and (b) the (Q_2, r_2)-plane, computed using (a) and the transformation defined by equations (21) and (22).

Using the linear transformation defined by the real parts of (21)-(22) we can redraw figure 10(a) in the (Q_2, r_2)-plane - figure 10(b). This makes comparison with the work of Clune and Knobloch [1, figure 5(b)] much easier, and shows the huge amount of structure which cannot be seen with only one bifurcation parameter but which is captured in a two-parameter unfolding. As the transformation between (μ_1, μ_2) and (Q_2, r_2) is far from orthogonal, the region of stability of Diagonal Rolls is squeezed almost to nothing, and there is a much larger region of chaotic behaviour, as investigated in section 4.4.

4.6 Bifurcations for larger ζ

Following on from the analysis of section 4.4 we can analyse the transverse stabilities of $\mathcal{S}_1$ and $\mathcal{S}_2$ and hence derive the bifurcation structure in a path

around the origin in the (μ_1, μ_2)-plane as ζ varies. This is summarised in figure 11. To the left of line a in figure 11 Standing Squares (SS) are the stable branch from the Hopf bifurcation. As discussed in section 4.3, to the right of line a this solution becomes quasiperiodic. By computing the transverse stability of all the primary solutions in the oscillatory subspace, we can obtain a *necessary* condition for the subspace as a whole to be transversely stable. This is indicated by the dotted line; above the dotted line the whole subspace $\mathcal{S}_1$ is certainly not transversely stable.

To the right of line b in figure 11 AR are stable in the oscillatory subspace, and to the right of line c both TR and AR are stable. The bifurcation structure at high ζ has also been explored in detail, but we will not present the results here.

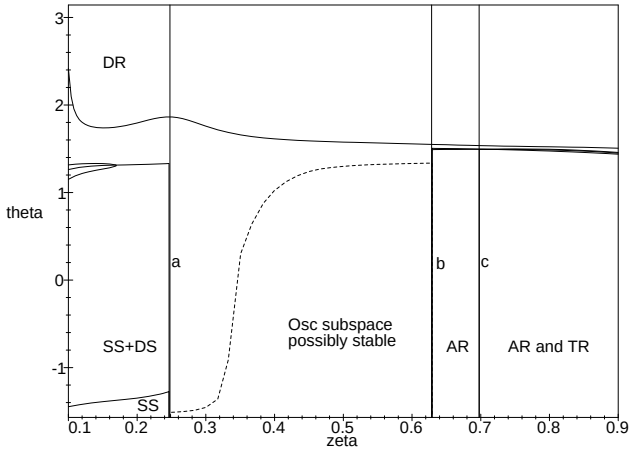

Fig. 11. Stable solutions for varying ζ in a circle around the origin. Because all bifurcations take place on straight (half-)lines passing thorough the origin, they are parametrised by $\theta = \tan^{-1}(\mu_2/\hat{\mu}_1)$. $\theta = -\pi/2$ is the initial Hopf bifurcation from the origin, and $\theta = \pi$ is the initial steady bifurcation from the origin. Only the first two bifurcations at most are shown. The meaning of the lines a, b and c is explained in the text. Note the much greater region of stability of AR at high ζ as opposed to SS at low ζ.

4.7 Numerical results

The analytical work of section 4.4 (and, by implication, the calculation of the normal form coefficients) was confirmed using a pseudospectral code for Boussinesq magnetoconvection developed by Cox and Matthews [22]. Figure 12 shows a numerically obtained instantaneous picture of the vertical velocity of the fluid layer at the mid-plane which agrees very well with that

obtained analytically (shown in figure 7), and is numerically well-converged.

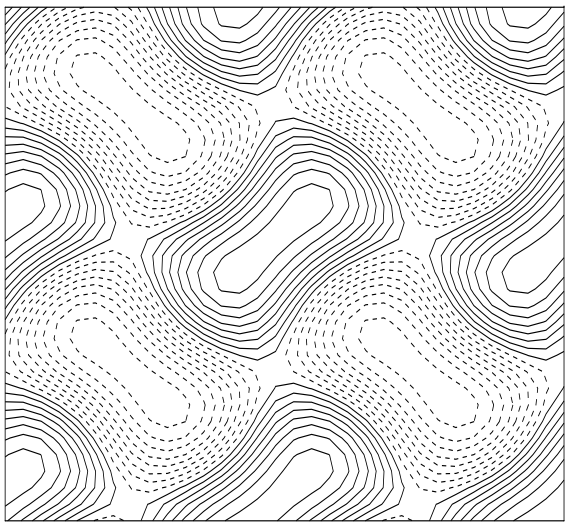

Fig. 12. SS+DS solution from the PDEs for Boussinesq magnetoconvection with $\zeta = 0.1$. $\hat{\mu}_1 = 5$, $\mu_2 = 10$ and $\epsilon = 0.1$ which corresponds to physical parameters $R = 1657.9$, $Q = 43.8$ and $\sigma = 0.0855$. The time step $\Delta t = 0.02$.

5 Analysis of the weakly non-Boussinesq equations for $\zeta = 0.1$

Non-Boussinesq effects introduce the quadratic terms with coefficients α_1 and ν_1. ν_1 is forced to be real by the symmetries, but α_1 may be complex. By rescaling the amplitudes we can see that only the ratio of these coefficients is important and, in addition, always ensure $\nu_1 > 0$. We will focus on two cases with very different dynamics: $\alpha_1 = \nu_1 > 0$ and $-\alpha_1 = \nu_1 > 0$. No new normal form symmetry is introduced by taking $\alpha_1 \in \mathbb{R}$ so these two cases are generic. Throughout this section we fix $\zeta = 0.1$ to enable comparison with the Boussinesq results.

In the analysis we find a wealth of different types of behaviour: we will only be interested in what happens very close to the origin in the (μ_1, μ_2)-plane: the stable behaviour may be very different to that of the Boussinesq problem, and it will accurately describe the behaviour of a non-Boussinesq fluid close to onset. Further from the origin we expect the problem to look more and more like the Boussinesq one we have already studied. The form of the behaviour in between is very complex and much less relevant to physical applications.

5.1 *Case 1:* $\alpha_1 = \nu_1 > 0$

The stable solutions in different regions of the (μ_1, μ_2)-plane were determined using AUTO, and a sketch of the results is given in figure 13.

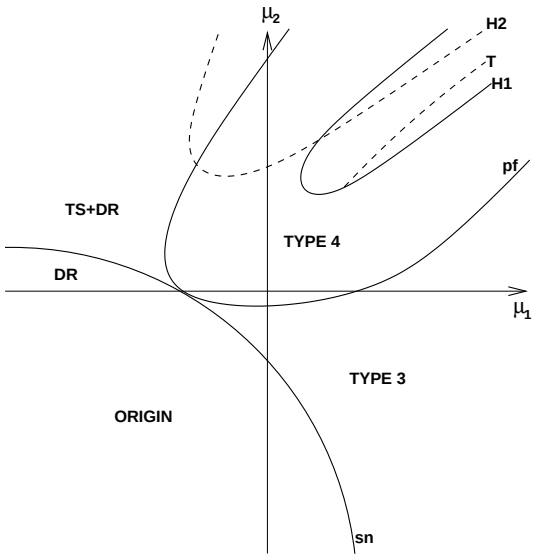

Fig. 13. Stable solutions in the (μ_1, μ_2)-plane for case 1 of the non-Boussinesq problem with $\zeta = 0.1$. The lines $H1$ and $H2$ indicate Hopf bifurcations from the type 4 solution. There is a subsequent secondary Hopf bifurcation to a triply-periodic solution of the full equations along the line marked T. The *Travelling Squares plus Diagonal Rolls* solution is indicated by TS+DR.

Near the origin type 4 solutions are stable, and near the negative μ_1-axis Diagonal Rolls are stable (as for the Boussinesq problem). Because of the quadratic terms the SS solution in the Boussinesq problem does not exist here ($\mathcal{S}_1$ is not an invariant subspace for the non-Boussinesq problem). Further away from the origin we see secondary bifurcations to quasiperiodic solutions, and then a chaotic region appears further out, but we do not find chaotic solutions near the origin. The stable type 3 solutions are created in a saddle-node bifurcation as we cross the line *sn* in figure 13, and these undergo a pitchfork bifurcation to type 4 solutions at the line *pf*. The determination of this line analytically is theoretically straightforward, but becomes algebraically very messy. It is not pursued here. There are many other bifurcations as we cross the μ_1 and μ_2 axes but they do not create stable solutions and are not shown.

As we go further from the origin, the type 3 solution - $SS+\{C \neq D\}$ - becomes closer and closer to an SS+DS solution, so 'at infinity' (corresponding to the limit $\alpha_1 \to 0$, $\nu_1 \to 0$) we recover the Boussinesq behaviour.

5.2 Case 2: $-\alpha_1 = \nu_1 > 0$

The normal form contains a large number of invariant subspaces. To give an idea of the complexity of case 2, we can find a subspace which contains all the dynamics of the 2:1 two-dimensional resonance problem studied by Armbruster, Guckenheimer and Holmes [23], Proctor and Jones [24] and Julien [25, chapter 2]. This includes the formation of robust homoclinic cycles. Moreover, this subspace is related by symmetry to three others, so there are four copies of these dynamics embedded in the problem.

Define the subspace $\mathcal{V}$ as being where A_1, B_1 and D are non-zero, and all other amplitudes are zero. This subspace is flow-invariant, and the dynamics are:

$$\dot{A}_1 = A_1[\mu_1 + \lambda_1|A_1|^2 + \lambda_3|B_1|^2 + \lambda_4|D|^2] + \alpha_1 D B_1 \tag{42}$$
$$\dot{B}_1 = B_1[\mu_1 + \lambda_1|B_1|^2 + \lambda_3|A_1|^2 + \lambda_4|D|^2] + \alpha_1 \bar{D} A_1 \tag{43}$$
$$\dot{D} = D[\mu_2 + \beta_1|D|^2 + \beta_3|A_1|^2 + \bar{\beta}_3|B_1|^2] + \nu_1 A_1 \bar{B}_1 \tag{44}$$

Writing the modes in terms of their moduli and arguments we find there is only one important phase difference; $\chi = \theta_{B_1} - \theta_{A_1} + \theta_D$. If we further assume that $|A_1| = |B_1| = A$ then we reduce this system to three real equations for A, $|D|$ (we will just write D for $|D|$) and χ:

$$\dot{A} = A[\mu_1 + (\lambda_1^r + \lambda_3^r)A^2 + \lambda_4^r D^2] + AD\alpha_1 \cos\chi \tag{45}$$
$$\dot{D} = D[\mu_2 + \beta_1 D^2 + 2\beta_3^r A^2] + \nu_1 A^2 \cos\chi \tag{46}$$
$$\dot{\chi} = -\Big(2\alpha_1 D + \nu_1 \frac{A^2}{D}\Big)\sin\chi \tag{47}$$

This is the system analysed by [23–25] in which a stable robust homoclinic cycle is formed. Numerical integrations of the full system in the quadrant $\mu_1 > 0$, $\mu_2 > 0$ and analytic investigation of (45)-(47) give support to the following scenario: a stable DR solution bifurcates from the origin at $\mu_2 = 0$ and then loses stability to a DR+TR solution. This periodic solution then undergoes a secondary Hopf bifurcation which is supercritical close to the origin, and subcritical further away. This periodic orbit (as it appears in (45)-(47)) then collides with the DR fixed point to create a robust cycle. This sequence of events is identical to that found in the 2:1 steady-state/steady-state mode interaction. The resulting bifurcation structure away from the origin is very complex. We also numerically find trajectories that cycle irregularly between the two DR fixed points ($C = 0$, $D \neq 0$) and ($C \neq 0$, $D = 0$). Near each fixed point the flow is locally expanding but the global contraction indicates the existence of a chaotic attractor.

What is much more analytically tractable (and does not occur in the 2:1 resonance problem) is the behaviour in the quadrant $\mu_1 > 0$, $\mu_2 < 0$ of the (μ_1, μ_2)-plane. As we cross from $\mu_1 < 0$ to $\mu_1 > 0$ with μ_2 fixed and negative we find that stable AR and SR solutions appear. This is due to the stabilising effect of the quadratic terms in (13)-(18). More interestingly, these two oscillatory solutions make the quadratic terms in the $\dot{C}$ and $\dot{D}$ equations vanish, so these two solutions will lose stability to perturbations in C and D along a straight line passing through the origin in exactly the same way as for the Boussinesq problem.

We summarise the regions of existence of these two unexpected solutions near the origin. There is a wealth of extra detail which is omitted: we concentrate on the central result that there are regions of the (μ_1, μ_2)-plane where these solutions exist and are stable.

5.2.1 Stable solutions from Alternating Rolls

An Alternating Roll solution is of the form $|A_1| = |A_2| = |B_1| = |B_2|$, $\psi = \pi$. It loses stability to an AR+DS solution when

$$\frac{\mu_2}{\mu_1} = \frac{2\beta_3^r - \nu_2}{\lambda_1^r + \lambda_2^r + 2\lambda_3^r - \alpha_2^r} \tag{48}$$

which defines a straight line passing through the origin in the (μ_1, μ_2)-plane labelled *pf1* in figure 14(a). By a usual perturbation argument we can also find where the AR solution becomes unstable to SCR+DS (*Standing Cross Roll plus Diagonal Squares*) solutions; these have the form $|A_1| = |A_2|$, $|B_1| = |B_2|$, $|C| = |D|$, $\phi_1 = \phi_2 = 0$, $\psi = \pi$). Let

$$\begin{aligned} &|A_1| = |A_2| = r_{AR} + u \qquad |B_1| = |B_2| = r_{AR} - u \\ &|C| = |D| = v \qquad\qquad\quad \phi_1 = \phi_2 = 0 \\ &\psi = \pi + \hat{\psi} \end{aligned} \tag{49}$$

and linearising in the small perturbations u, v and $\hat{\psi}$ (dropping the hat):

$$\begin{pmatrix} \dot{u} \\ \dot{v} \\ \dot{\psi} \end{pmatrix} = \begin{pmatrix} \mu_1 + r_{AR}^2(3f^r + 4\lambda_3^r + \alpha_2^r) & 0 & r_{AR}^3\alpha_2^i \\ 0 & \mu_2 + r_{AR}^2(4\beta_3^r + 2\nu_2) & \nu_1 r_{AR}^2 \\ -8r_{AR}(f^i + \alpha_2^i) & -8\alpha_1 & 4\alpha_2^r r_{AR}^2 \end{pmatrix} \begin{pmatrix} u \\ v \\ \psi \end{pmatrix}$$

The AR solution is unstable to SCR+DS perturbations when this matrix has a zero eigenvalue. This defines the line *pf2* in figure 14(a).

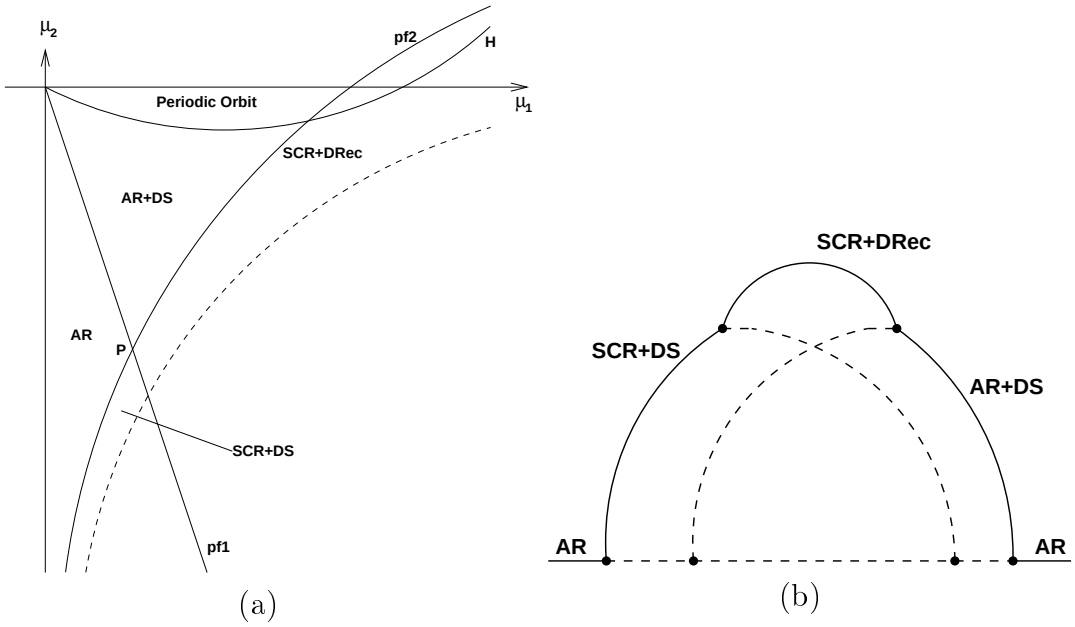

Fig. 14. (a) Incomplete sketch of the (μ_1, μ_2)-plane showing the region of stable Alternating Roll (AR) solutions for case 2 of the non-Boussinesq problem with $\zeta = 0.1$. To the right of the dotted line neither SCR+DS nor SCR+DRec (*Standing Cross Rolls plus Diagonal Rectangles*) exist - they disappear in saddle-node bifurcations. (b) Bifurcation diagram following a circle anticlockwise around the point P.

5.2.2 Stable solutions from Standing Rolls

Similarly, Standing Roll solutions are of the form $|A_1| = |A_2|$, $|B_1| = |B_2| = 0$. Numerical investigations show that they also lose stability in two ways. As in the case of Alternating Rolls we can apply the usual perturbation arguments to derive analytic expressions (at least implicitly) for the location of these bifurcation curves. The curve *H1* in figure 15 is the locus of a Hopf bifurcation from Standing Rolls. There is also a pitchfork bifurcation to a *Standing Rolls plus Diagonal Squares* solution along the line *pf*. The point *TB* where these two lines *H1* and *pf* meet is a Takens-Bogdanov point; a complete bifurcation diagram will include all the other bifurcations near the *TB* point.

In conclusion, even though the Boussinesq problem is dominated by solutions based on Standing Squares, a small amount of compressibility or another non-Boussinesq effect can introduce very different stable solutions.

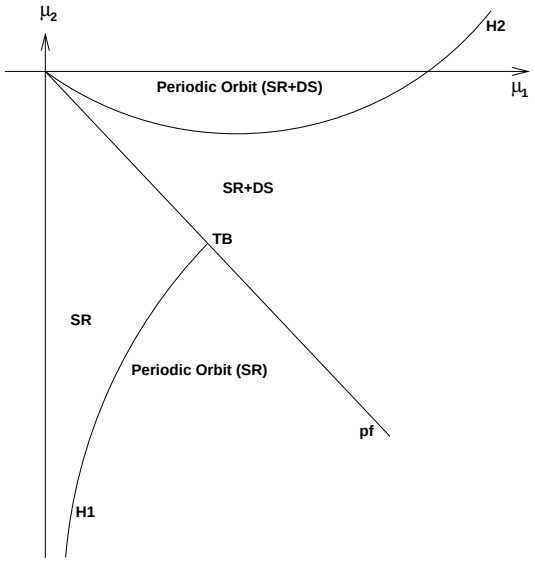

Fig. 15. Incomplete sketch of the (μ_1, μ_2)-plane showing the region of stable Standing Rolls (SR) for case 2 of the non-Boussinesq problem with $\zeta = 0.1$. Along the curve $H1$ there is a Hopf bifurcation from the SR solution, and along the curve $H2$ there is a Hopf bifurcation from the SR+DS solution.

6 Discussion and conclusions

In this paper we have investigated the stable periodic and quasiperiodic solutions near a codimension 2 point in an idealised magnetoconvection problem. There are several obvious deficiencies in the approach: restricting the problem to a periodic lattice is essential to ensure the centre manifold is finite-dimensional, but it means we cannot find the stability of these patterns to perturbations which do not lie on the lattice (e.g. hexagonal patterns), and we have not investigated stability to modulational disturbances.

This analysis has only a local validity around the codimension 2 point: by restricting solutions to other square lattices we can investigate mode interactions where the ratio of wavenumbers is not $1 : \sqrt{2}$, but other irrational ratios. The $1 : \sqrt{2}$ resonance will have a great influence on a complete description of the transition from steady to oscillatory convection because it is such a strong resonance, affecting the amplitude equations at third order.

This transition from steady to oscillatory forms of convection completes the analysis of Clune and Knobloch [1]. Although the most unstable wavenumber jumps as we cross the CT line, by introducing a second bifurcation parameter as we have done here, it is possible to build up a coherent, continuous picture of this smooth transition.

Even ignoring non-Boussinesq effects, it is a very complex transition. We have seen examples of chaotic sets created in each of the three common ways,

namely the breakup of a torus, through a period-doubling cascade of periodic orbits, and from a homoclinic connection at a fixed point. This complexity is the reason for concentrating only on stable objects, and not attempting to present a complete bifurcation structure. The continuation and bifurcation package AUTO [14] was used in conjunction with analytic techniques and symmetry arguments: these three approaches complement each other.

The non-Boussinesq analysis is much more difficult, and very little can be done analytically. In case 1, where α_1 and ν_1 have the same sign the behaviour near the origin is qualitatively similar to that in the Boussinesq problem. However, case 2 (α_1 and ν_1 have opposite signs) contains regions of stable AR and SR which are not seen in the Boussinesq case. Interestingly, when the oscillatory modes have the form of Alternating Rolls, ie $(A_1, A_2, B_1, B_2) = (\mathbf{z}, \mathbf{z}, i\mathbf{z}, i\mathbf{z})$ the quadratic terms $A_1\bar{B}_2 + B_1\bar{A}_2$ and $A_1\bar{B}_1 + B_2\bar{A}_2$ in the $\dot{C}$ and $\dot{D}$ equations are identically zero. This simplifies some of the analysis in case 2. The fact that a large qualitative change in behaviour can occur between the Boussinesq and non-Boussinesq problems is also interesting. Numerical studies of 3D compressible magnetoconvection in the oscillatory regime have demonstrated a strong preference for AR and TR over the other periodic planforms [26, section 5.2].

The appearance of drifting solutions has been observed in numerical experiments on compressible magnetoconvection and and has been analysed theoretically [2]. The theoretical framework of bifurcations with continuous and spatio-temporal symmetries which explains the occurrence of these novel solutions is very general [19,20], and finds many other applications, for example the appearance of 'superlattice' patterns in Faraday-wave experiments [17,18].

The $1 : \sqrt{2}$ interaction also occurs in rotating thermal convection. Work on this problem is in progress [27]: the required physical parameters (Prandtl number and Taylor number) can be obtained experimentally, so direct comparisons between theory and experiment could be made.

Acknowledgements

I have benefited greatly from discussions with Rebecca Hoyle, Robert MacKay, Michael Proctor and Alastair Rucklidge. The possibility of mode interactions of this type was first noticed during numerical experiments on Boussinesq magnetoconvection by Laurent Leboucher (unpublished). I would like to thank Steve Cox and Paul Matthews for making their code for Boussinesq magnetoconvection available [22]. I also acknowledge many useful comments on the manuscript by an anonymous referee. This work was funded by the EPSRC.

Appendix

By writing the complex amplitudes as $A_1 = \tilde{A}_1 e^{i\theta_{A_1}}$, $C = \tilde{C} e^{i\theta_C}$ etc we can rewrite the equations (13)-(18) as evolution equations for the moduli and phases of the six complex variables. These translational symmetries mean we can eliminate three of the phase variables, and the moduli equations depend on only three combinations of the phase variables. Thus we can form a reduced set of 9 equations; six moduli and three phase equations. Define

$$\begin{aligned}
\phi_1 &= \theta_{B_2} - \theta_{B_1} + \theta_C - \theta_D \\
\phi_2 &= \theta_{A_2} - \theta_{A_1} + \theta_C + \theta_D \\
\psi &= \theta_{B_1} + \theta_{B_2} - \theta_{A_1} - \theta_{A_2}
\end{aligned}$$

and, dropping the tildes on the moduli variables, the reduced equations for the Boussinesq problem are

$$\begin{aligned}
\dot{A}_1 = {} & A_1\Big[\mu_1 + \lambda_1^r A_1^2 + \lambda_2^r A_2^2 + \lambda_3^r (B_1^2 + B_2^2) + \lambda_4^r (C^2 + D^2)\Big] \\
& + A_2 B_1 B_2 (\alpha_2^r \cos\psi - \alpha_2^i \sin\psi) + A_2 CD(\alpha_3^r \cos\phi_2 - \alpha_3^i \sin\phi_2) \qquad (50)
\end{aligned}$$

$$\begin{aligned}
\dot{A}_2 = {} & A_2\Big[\mu_1 + \lambda_1^r A_2^2 + \lambda_2^r A_1^2 + \lambda_3^r (B_1^2 + B_2^2) + \lambda_4^r (C^2 + D^2)\Big] \\
& + A_1 B_1 B_2 (\alpha_2^r \cos\psi - \alpha_2^i \sin\psi) + A_1 CD(\alpha_3^r \cos\phi_2 + \alpha_3^i \sin\phi_2) \qquad (51)
\end{aligned}$$

$$\begin{aligned}
\dot{B}_1 = {} & B_1\Big[\mu_1 + \lambda_1^r B_1^2 + \lambda_2^r B_2^2 + \lambda_3^r (A_1^2 + A_2^2) + \lambda_4^r (C^2 + D^2)\Big] \\
& + B_2 A_1 A_2 (\alpha_2^r \cos\psi + \alpha_2^i \sin\psi) + B_2 CD(\alpha_3^r \cos\phi_1 - \alpha_3^i \sin\phi_1) \qquad (52)
\end{aligned}$$

$$\begin{aligned}
\dot{B}_2 = {} & B_2\Big[\mu_1 + \lambda_1^r B_2^2 + \lambda_2^r B_1^2 + \lambda_3^r (A_1^2 + A_2^2) + \lambda_4^r (C^2 + D^2)\Big] \\
& + B_1 A_1 A_2 (\alpha_2^r \cos\psi + \alpha_2^i \sin\psi) + B_1 CD(\alpha_3^r \cos\phi_1 + \alpha_3^i \sin\phi_1) \qquad (53)
\end{aligned}$$

$$\begin{aligned}
\dot{C} = {} & C\Big[\mu_2 + \beta_1 C^2 + \beta_2 D^2 + \beta_3^r (A_1^2 + B_1^2 + A_2^2 + B_2^2)\Big] \\
& + \nu_2 (B_1 B_2 D \cos\phi_1 + A_1 A_2 D \cos\phi_2) \qquad (54)
\end{aligned}$$

$$\begin{aligned}
\dot{D} = {} & D\Big[\mu_2 + \beta_1 D^2 + \beta_2 C^2 + \beta_3^r (A_1^2 + B_1^2 + A_2^2 + B_2^2)\Big] \\
& + \nu_2 (B_1 B_2 C \cos\phi_1 + A_1 A_2 C \cos\phi_2) \qquad (55)
\end{aligned}$$

$$\begin{aligned}
\dot{\phi}_1 = {} & A_1 A_2 \Big(\frac{B_1}{B_2} - \frac{B_2}{B_1}\Big)(\alpha_2^i \cos\psi - \alpha_2^r \sin\psi) + (\lambda_1^i - \lambda_2^i - 2\beta_3^i)(B_2^2 - B_1^2) \\
& + \frac{B_1 CD}{B_2}(\alpha_3^i \cos\phi_1 - \alpha_3^r \sin\phi_1) - \frac{B_2 CD}{B_1}(\alpha_3^r \sin\phi_1 + \alpha_3^i \cos\phi_1)
\end{aligned}$$

$$+\nu_2\Big[A_1A_2\Big(\frac{C}{D}-\frac{D}{C}\Big)\sin\phi_2 - B_1B_2\Big(\frac{C}{D}+\frac{D}{C}\Big)\sin\phi_1\Big] \tag{56}$$

$$\begin{aligned}\dot{\phi}_2 = {} & B_1B_2\Big(\frac{A_1}{A_2}-\frac{A_2}{A_1}\Big)(\alpha_2^r\sin\psi+\alpha_2^i\cos\psi)+(\lambda_1^i-\lambda_2^i-2\beta_3^i)(A_2^2-A_1^2)\\ & +\frac{A_1CD}{A_2}(\alpha_3^i\cos\phi_2-\alpha_3^r\sin\phi_2)-\frac{A_2CD}{A_1}(\alpha_3^r\sin\phi_2+\alpha_3^i\cos\phi_2)\\ & +\nu_2\Big[B_1B_2\Big(\frac{C}{D}-\frac{D}{C}\Big)\sin\phi_1 - A_1A_2\Big(\frac{D}{C}+\frac{C}{D}\Big)\sin\phi_2\Big]\end{aligned} \tag{57}$$

$$\begin{aligned}\dot{\psi} = {} & A_1A_2\Big(\frac{B_1}{B_2}+\frac{B_2}{B_1}\Big)(\alpha_2^i\cos\psi-\alpha_2^r\sin\psi)-B_1B_2\Big(\frac{A_1}{A_2}+\frac{A_2}{A_1}\Big)(\alpha_2^i\cos\psi+\alpha_2^r\sin\psi)\\ & +CD\alpha_3^i\Big[(\frac{B_1}{B_2}+\frac{B_2}{B_1})\cos\phi_1-(\frac{A_1}{A_2}+\frac{A_2}{A_1})\cos\phi_2\Big]\\ & +CD\alpha_3^r\Big[(\frac{B_2}{B_1}-\frac{B_1}{B_2})\sin\phi_1+(\frac{A_1}{A_2}-\frac{A_2}{A_1})\sin\phi_2\Big]\\ & +(\lambda_1^i+\lambda_2^i-2\lambda_3^i)(B_1^2+B_2^2-A_1^2-A_2^2)\end{aligned} \tag{58}$$

References

[1] T. Clune and E. Knobloch, Pattern selection in three-dimensional magnetoconvection. *Physica D* **74** (1994) 151–176.

[2] A.M. Rucklidge and M. Silber, Bifurcations of periodic orbits with spatio-temporal symmetries. *Nonlinearity* **11**, (1998) 1435–1455.

[3] M. Silber and E. Knobloch, Hopf bifurcation on a square lattice. *Nonlinearity* **4**, (1991) 1063–1106.

[4] G. Dangelmayr, Steady-state mode interactions in the presence of $O(2)$ symmetry. *Dyn. Stab. Syst.* **1** (1996) 159–185.

[5] A. Hill and I.N. Stewart, Hopf–steady-state mode interactions with $O(2)$ symmetry. *Dyn. Stab. Syst.* **6** (1991) 149–171.

[6] M.R.E. Proctor and N.O. Weiss, Magnetoconvection. *Rep. Prog. Phys.* **45**, (1982) 1317–1379.

[7] G. Dangelmayr and E. Knobloch, The Takens-Bogdanov bifurcation with $O(2)$ symmetry. *Phil. Trans. R. Soc. Lond. A* **322** (1987) 243–279.

[8] M.R.E. Proctor and P.C. Matthews, $\sqrt{2}$: 1 Resonance in non-Boussinesq convection. *Physica D* **97**, (1996) 229–241.

[9] Y.Y. Renardy, M. Renardy and K. Fuijmura, Takens-Bogdanov bifurcation on the hexagonal lattice for double-layer convection. *Physica D* **129**, (1999) 171–202.

[10] J.H.P. Dawes, Stable quasiperiodic solutions in the Hopf bifurcation with $D_4 \ltimes T^2$ symmetry. *to appear in Physics Letters A*

[11] S. Chandrasekhar, *Hydrodynamic and Hydromagnetic Stability.* Oxford University Press (1961), republished by Dover Publications, Inc. (1981)

[12] B. Dionne, M. Silber and A.C. Skeldon, Stability results for steady, spatially periodic planforms. *Nonlinearity* **10**, (1997) 321–353

[13] M. Golubitsky, I.N. Stewart and D.G. Schaeffer, *Singularities and Groups in Bifurcation Theory. Volume II.* Springer, Applied Mathematical Sciences Series **69** (1988).

[14] E. Doedel, A. Champneys, T. Fairgrieve, Y. Kusnetsov, B. Sandstede and X. Wang, *AUTO97: Continuation and bifurcation software for ordinary differential equations.* Available via FTP from directory `pub/doedel/auto` at `ftp.cs.concordia.ca` (1997)

[15] P.C. Matthews and A.M. Rucklidge, Travelling and standing waves in magnetoconvection. *Proc. R. Soc. Lond. A.* **441**, (1993) 649–658

[16] J. Swift, Hopf bifurcation with the symmetry of a square. *Nonlinearity* **1**, (1988) 333–377

[17] M. Silber and M.R.E. Proctor, Nonlinear competition between small and large hexagonal patterns. *Phys. Rev. Lett.* **81**, (1998) 2450–2454

[18] D.P. Tse, A.M. Rucklidge, R.B. Hoyle and M. Silber, Secondary instabilities of standing hexagons in a Faraday wave experiment. *submitted to Physica D*

[19] J.S.W. Lamb and I. Melbourne, Bifurcation from periodic solutions with spatiotemporal symmetry, in *Pattern Formation in Continuous and Coupled Systems* eds M. Golubitsky, D. Luss and S.H. Strogatz. New York, Springer. (1999) 175–192

[20] C. Wulff, J.S.W. Lamb and I. Melbourne, Bifurcation from relative periodic orbits. *preprint*

[21] J.F. Cornwell, *Group Theory in Physics. Volume 1.* Academic Press. (1984)

[22] S.M. Cox and P.C. Matthews, A pseudospectral code for convection with an analytic / numerical implementation of horizontal boundary conditions. *Int. J. Numer. Meth. Fluids* **25** (1997) 151–166

[23] D. Armbruster, J. Guckenheimer and P. Holmes, Heteroclinic cycles and modulated travelling waves in systems with O(2) symmetry. *Physica D* **29** (1987) 257–282

[24] M.R.E. Proctor and C.A. Jones, The interaction of two spatially resonant patterns in thermal convection. Part 1: Exact 1:2 resonance. *J. Fluid Mech.* **188**, (1988) 301–335

[25] K.A. Julien, *Strong Spatial Resonance in Convection.* PhD thesis, University of Cambridge (1991)

[26] P.C. Matthews, M.R.E. Proctor and N.O. Weiss, Compressible magnetoconvection in three dimensions: planforms and nonlinear behaviour. *J. Fluid Mech.* **305**, (1995) 281–305.

[27] J.H.P. Dawes, Pattern selection in oscillatory rotating convection. *in preparation*